AD670731

DECOMPOSITION CHARACTERISTICS OF NITRATE ESTER MONOPROPELLANTS

By G. A. Yanyecic

Technical Memorandum
File No. TM 705.9161-03
January 17, 1968
Contract NOw 65-0123-d
Copy No. 10

THIS DOCUMENT HAS BEEN APPROVED
FOR PUBLIC RELEASE AND SALE;
ITS DISTRIBUTION IS UNLIMITED

The Pennsylvania State University
Institute for Science and Engineering
ORDNANCE RESEARCH LABORATORY
University Park, Pennsylvania

DDC
RECEIVED
JUN 27 1968

NAVY DEPARTMENT · NAVAL ORDNANCE SYSTEMS COMMAND

Reproduced by the
CLEARINGHOUSE
for Federal Scientific & Technical
Information Springfield Va. 22151

100

UNCLASSIFIED

Abstract: A theoretical and experimental investigation was made of the combustion characteristics of nitrate ester droplets, including propylene glycol dinitrate, ethyl nitrate and n-propyl nitrate, at various ambient gas temperatures and pressures. Measurements were made of droplet diameter and temperature during combustion. At high pressures, the droplet ignited early in its heat-up period at a more or less fixed liquid temperature. At low pressures, the droplet ignited as its temperature approached the wet bulb temperature. A simplified theoretical model was found to give an adequate correlation of the ignition time in both regimes. A combustion model was formulated in studying the burning rates of the droplets. The model includes the effect of conviction on the burning rate. This model was found to be in fair agreement with the data.

* * *

This thesis was written on research work performed under the direction of Dr. G. M. Faeth in the Department of Mechanical Engineering.

UNCLASSIFIED

TABLE OF CONTENTS

LIST OF FIGURES

LIST OF FIGURES

NOMENCLATURE

A	Pre-exponential term
A_R	Surface area
a	Grouping of terms ($r_s^2 \dot{m}_s'' C_p/K$)
B	Dimensionless radiation absorption coefficient
C_p	Specific heat at constant pressure (BTU/lb ^oR)
C_i	Integration constants, i = 1, 4 (^oF)
d	Diameter (inches)
E	Activation energy (K cal/mol)
Gr	Dimensionless Grashof number
g	Acceleration of gravity (ft/sec^2)
h	Enthalpy (BTU/lb)
h_c	Convection heat transfer coefficient (BTU/hr ft^2 ^oF)
K	Thermal conductivity (BTU/hr ft ^oF)
k	Specific reaction rate constant
L	Latent heat (BTU/lb)
ℓ_1	Minor axis of ellipsoid (inches)
ℓ_2	Major axis of ellipsoid (inches)
m	Mass (lbm)
N_u	Dimensionless Nusselt number
n	Reaction order (dimensionless)
P	Pressure (atmospheres)

Pr	Dimensionless Prandtl number
Q	Dimensionless heat of reaction ($\Delta H_R / C_p T_\infty$)
$\dot{q}$	Heat transfer rate (BTU/hr)
R_o	Universal gas constant
r	Radial distance
S	Stefan-Boltzmann constant (BTU/hr ft^2 $^oR^4$)
T	Temperature (^oR)
t	Time (seconds)
V	Volume (ft^3)
v	Velocity (ft/sec)
Y_f	Mass fraction of fuel
α	Dimensionless latent heat ($L/C_p T_\infty$)
β	A constant
ΔH_R	Heat of reaction (BTU/lb)
δ	Boundary layer thickness (ft)
η	Dimensionless radial distance (2r/d)
θ	Dimensionless temperature ratio (T/T_∞)
θ_R	Activation energy ratio ($E/R T_\infty$)
μ	Absolute viscosity (lb/ft sec)
ν	Dimensionless radial velocity
ρ	Density (lb/ft^3)
σ	Dimensionless radius (r/r_s)

Subscripts and superscripts:

ℓ	Liquid
g	Gas
o	Initial
∞	Free stream
s	Drop surface
f	Flame
R	Zone of reactants
P	Zone of products
"	Per unit area

CHAPTER I

INTRODUCTION

1.1 General Statement of the Problem

The majority of liquid propellants employed in non-airbreathing propulsion and power systems are bipropellants. In a bipropellant system, separate fuel and oxidizer streams enter the combustion chamber where they react to yield high temperature gaseous products.

A second class of liquid fuels consists of monopropellants. A monopropellant is a single fluid capable of undergoing an exothermic decomposition to yield high temperature gaseous products. With a monopropellant system, only a single propellant stream enters the combustion chamber. A familiar example of a liquid monopropellant is nitroglycerine.

Liquid monopropellants possess certain inherent advantages over conventional bipropellant fuels. They can be stored in a single tank, thus simplifying refueling operations. Most of these propellants are liquids at room temperature so that there is no need for cryogenic fuel storage. They require only a single fuel pump and injector which simplifies the design of the fuel feed system. In addition, the ambient temperature variation results in

density changes which can affect the mixture ratio of bipropellant systems. This problem is not present in monopropellant systems. The result of using monopropellant systems is a simplification of overall design with a resulting increase in reliability and reduction in cost.

On the other hand, monopropellants have certain disadvantages that tend to limit their application. In general, their performance is inferior to bipropellant systems and, in terms of present technology, they are more costly. Thus, they are not good competitors with bipropellants for large booster applications where performance is critical.

These characteristics make monopropellant fuels desirable for use in certain non-airbreathing devices such as small thrusters, hot gas generators and small power systems. Since most power systems must respond to varying loads, the need to control only a single propellant flow is a real advantage.

To design a combustor for these fuels, one must have an understanding of fuel spray characteristics and the behavior of the atomized fuel at elevated pressure and temperature. The combustor must be of such dimensions to allow the fuel droplets to vaporize, ignite and decompose before the gases leave the combustion chamber. Rational design of such combustion chambers requires a knowledge of the combustion characteristics of the individual propellant droplets. Thus, the purpose of this investigation is to determine the effects

of variation in temperature, pressure and drop size on the ignition and decomposition of single droplets of selected monopropellant fuels.

1.2 Previous Studies

In recent years, droplet combustion studies (References 1-5, to name a few) have formed a new area of combustion research. Bipropellant droplet studies have been more numerous than monopropellant studies since the majority of liquid fuels have been bipropellants.

Priem and Heidmann[6] developed a widely accepted method of applying droplet vaporization theory to the design of a combustion chamber. They considered propellant vaporization to be the rate-controlling parameter and developed equations and design charts to determine combustor dimensions and efficiencies. The availability of bipropellant vaporization data from droplet studies has enabled this method to be applied over a wide range of fuels. It would be desirable to have monopropellant vaporization data from a droplet study which, at present, is practically non-existent to further extend the applicability of this method.

A step in the direction of understanding monopropellant systems was the investigation of gaseous monopropellant decomposition. Adams and Bawn[7] studied the gaseous decomposition of ethyl nitrate at temperatures of 180° to 215°C. Their technique was to rapidly place

the fuel vapor into a bulb maintained at constant temperature. The course of the reaction was then followed by observing the variation of pressure within the bulb. The reaction was found to be first-order and the values for the rate constants in the first-order Arrhenius expression were determined. A mechanism is suggested in which the first step is the breaking of the O-N bond which releases the NO_2 group.

Phillips[3] investigated the decomposition of gaseous nitromethane at temperatures between 150° and 240°C. He used a mass spectrometer to determine component concentrations and suggested a mechanism by which the NO group is first released. In addition, he gives the first-order rate constants for the temperature dependence on the rate of loss of nitromethane.

Levy[10] also studied the thermal decomposition of gaseous ethyl nitrate, but at 151° to 201°C and pressures of a few cm. He used the infrared and visible spectrophotometric technique to detect the components produced. From his measurements, he determined the kinetic constants and also suggested the release of the NO_2 group as the first step in the mechanism. In addition, he determined rate constants for the first-order reaction and compared his results with those of Adams and Bawn[7].

One of the first liquid monopropellant droplet studies was conducted by Barrere and Moutet[12]. Their apparatus consisted of an electrically heated furnace mounted on rails with a window at one

end and an opening on the other. The furnace could be flooded with nitrogen providing an inert atmosphere which simulated combustor conditions. The drop was mounted on a quartz probe and the drop size was recorded with a movie camera. Barrere tested a variety of monopropellants at temperatures between 1000° and 1600°F and diameters of 0.030 to 0.080 inches. The apparatus was limited to atmospheric pressure. From the film, Barrere converted the elliptical appearance of the droplet into an equivalent spherical diameter and plotted diameter squared versus time. The slope of the resulting curve is the burning rate constant. Variations of burning rate constant with chamber temperature are presented for several fuels including ethyl nitrate and normal propyl nitrate. Barrere concentrated on the steady burning period and did not study the ignition period preceding the steady state combustion. Hence, it would be desirable to extend the pressure range and to obtain ignition results for these fuels. This would result in a better understanding of droplet behavior over a larger portion of their lifetime.

Rosser[13] studied the steady evaporation rate of several monopropellants by simulating the drop with a porous alumina sphere. The sphere was centered in a cylindrical pyrex chamber. A flow of gas at room temperature was maintained past the sphere. The sphere was internally supplied with liquid monopropellant which was accurately metered. After the propellant was introduced to the

sphere, it was ignited by an electric spark. Then, the flow rate was adjusted so that the sphere was just wetted, neither dripping excess fuel nor becoming dry. The flow rate at the balance point was just equal to the rate consumed and this was the measured quantity. Rosser found that he could not obtain visible decomposition flames unless oxygen was admitted to the chamber. Hence, his results are more applicable to bipropellant combustion and do not represent true decomposition. A test of this nature considers only the steady burning period and again tells us nothing about ignition. Since the experiment was conducted at atmospheric pressure, the effect of pressure variations could not be determined. This would be desirable to more nearly simulate combustor conditions.

In a study which directly preceded this investigation, Karhan[14] studied the ignition and combustion of a liquid monopropellant. His apparatus consisted of an electrically heated furnace mounted on vertical guide rods. The droplet was mounted on either a quartz probe or the junction of a chromel-alumel thermocouple. He employed a high speed movie camera to record the drop size and the entire apparatus, except the camera, was enclosed in a pressure vessel. The vessel could be evacuated and filled with a variety of gases. He could operate with a test temperature up to 1800^{o}F and pressures of 0.1 to 40 atmospheres. The drop

diameter was variable between 0.020 and 0.080 inches. With this apparatus, he could obtain ignition and decomposition data at various pressures.

Karhan developed a simple heat-up analysis to predict ignition times. He noted that ignition often occurred as the droplet temperature approached its equilibrium or wet bulb temperature (the temperature where the heat transferred to the droplet is completely utilized for the heat of vaporization of the vapor leaving the droplet). He also found, in agreement with others, that the wet bulb temperature was below but reasonably close to the boiling temperature of the fluid at the total pressure of the test. Thus, he computed the time required for ignition by calculating the time required for the droplet to heat up from its initial temperature to its boiling temperature. The effect of evaporation on the heat-up of the droplet was neglected. He found that the ignition times thus calculated agree with experimental ignition times at low pressure but fail at high pressure. Since he used only one fuel, it would be desirable to extend his heat-up theory to more fuels and also account for the disagreement at high pressures.

A combustion model presented by Williams[15] was employed by Karhan in an attempt to correlate his measured burning rate data. The analysis considers the steady burning period and involved several assumptions:

1) The reaction takes place in a thin spherical shell surrounding the droplet. This is the so-called "flame surface" approximation.
2) The drop temperature is const ..
3) The flame is spherically symmetrical and natural convection is neglected.
4) Thermal diffusion is neglected.
5) Quasi-steady burning is considered.
6) All gases obey the ideal gas equation of state, the total pressure is constant and all gas properties are constant.

Using this analysis, Karhan found that unrealistically large values of thermal conductivity were needed in order for the activation energy of the reaction to be reasonable. Karhan suggested several possible reasons for the dilemma. First, the thin flame model may not truly represent the heat release process. A flame of finite thickness would result in lower flame temperatures and lower mass transfer rates. Secondly, Faeth[9] has shown that nonadiabatic monopropellant flames are particularly vulnerable to convection effects. Thus, Karhan suggested that natural convection could cause larger heat losses from the flame resulting again in lower transfer rates. The effect of lower transfer rates could reduce the abnormally large effective thermal conductivities necessary to obtain reasonable activation energies. Hence, it would be desirable

to investigate the underlying assumptions of Williams' analysis in an attempt to correlate measured burning rates with the predicted values and to apply the model to additional fuels.

1.3 Specific Statement of the Problem

From the previous discussion, it is evident that future studies of the ignition and combustion of monopropellant droplets would be desirable. The areas least understood at the present time center around the characteristics affecting the preignition period and droplet burning parameters at elevated pressures. With this in mind, the objectives of the present study were:

1) To check the heat-up theory of Karhan when applied to several other monopropellants.
2) To investigate the discrepancy between experimental and theoretical ignition delay times in the high pressure region.
3) To modify the combustion model to include natural convection effects.
4) To check the combustion model thus modified on several other monopropellants.

The fuels used in this study were propylene glycol dinitrate, ethyl nitrate, nitromethane and normal propyl nitrate, hereafter referred to as PGDN, EN, NM and NPN, respectively. The chemical formulas are shown in Appendix B.

CHAPTER II

EXPERIMENTAL APPARATUS, PROCEDURE AND DATA

2.1 Experimental Apparatus

The apparatus used was very similar to that of Karhan,[14] the requirements being:

a) To provide a means of rapidly immersing a monopropellant droplet in a high temperature gas to simulate a droplet breaking out of a spray in a combustion chamber.

b) To provide a facility to evacuate the air and introduce a variety of gases as the atmosphere.

c) To operate over an extended pressure range of 0.1 to 40 atmospheres.

d) To operate over a range from room temperature to 1800°F.

e) To record continuously and simultaneously the temperature of liquid and gas phase and diameter of droplet.

The external apparatus, Figure 2.1, consisted first of a base mounted to the floor by steel angles. The top cover was secured to the base by twelve 1-1/2 inch bolts and an "O" ring was installed between the cover and base to permit pressurization. The cover could be raised and lowered by a small hand winch. A flexible hose was attached to the cover and led to the evacuation pump, pressure

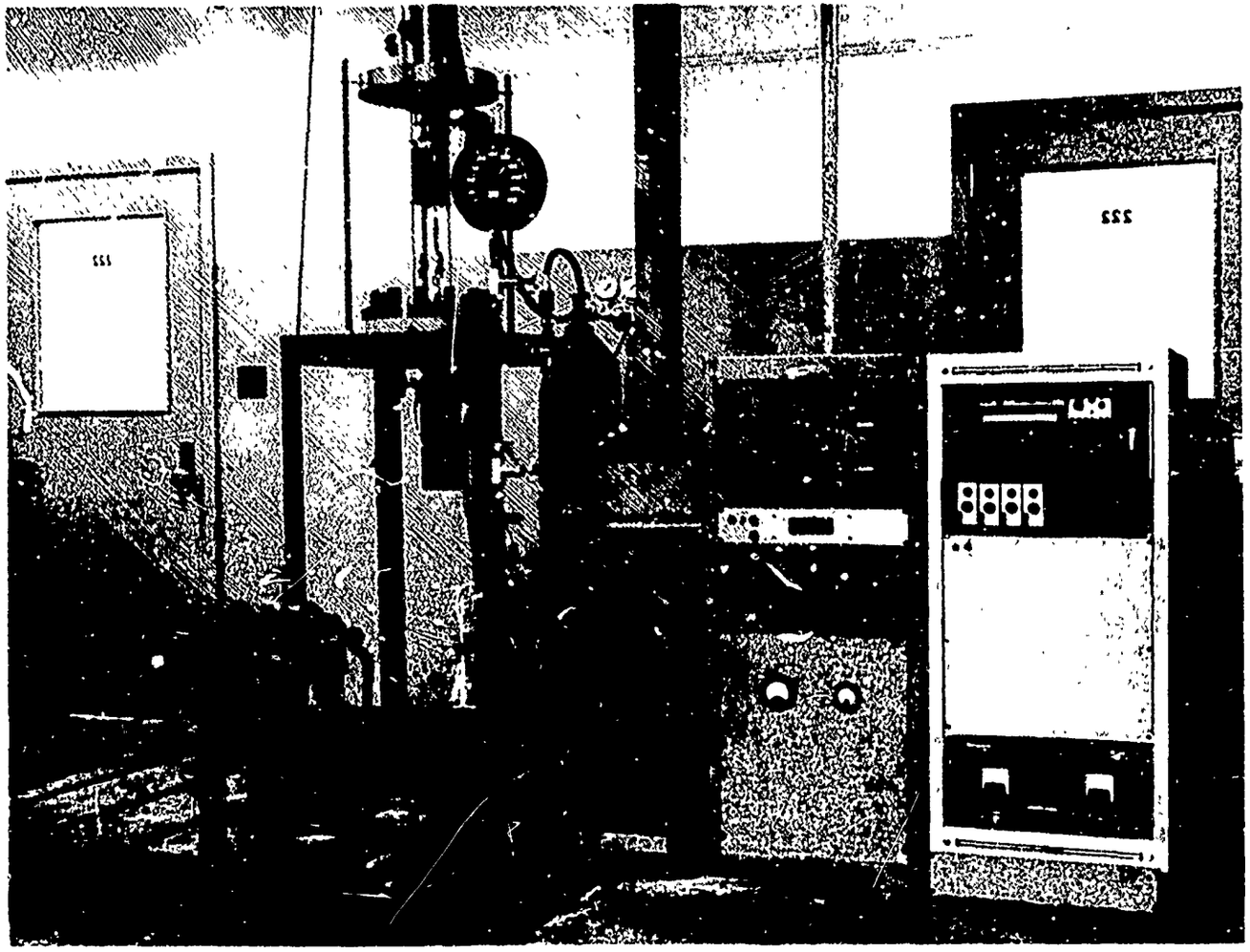

Figure 2.1 External Apparatus

gages and high pressure gas supply. There was a small window on the cover to permit visual inspection of the droplet prior to the initiation of the test. In addition, the cover was fitted with an access screw plug 3/8-inch in diameter and located 6-7/16 inches above the top edge of the base. This permitted entry to the chamber with a probe for mounting the droplet. The droplet could not be mounted prior to lowering the cover since the fuels used evaporated rapidly even at room temperatures. The base was fitted with a window two inches in diameter for photographic purposes and pressure seals to electrically connect the internal and external leads. A 16 mm Fastair movie camera was mounted under the base. The camera was operated at speeds of approximately 100 frames per second and incorporated an internal timing marker to give a running calibration of film speed.

The internal apparatus, Figure 2.2, can be broken down into three sections: the upper chamber, the furnace and the lower chamber. In the upper chamber, a Westinghouse W-47 light bulb was mounted to supply background illumination for the camera. The light was powered by two series-connected six-volt batteries.

The next section consisted of an electrically heated furnace mounted on four vertical guide rods. The furnace was held in the top position by a 28-gage nichrome wire, 2-1/2 inches long, connected to two terminal posts. The furnace was released to fall over th droplet by passing a high current through the wire, causing

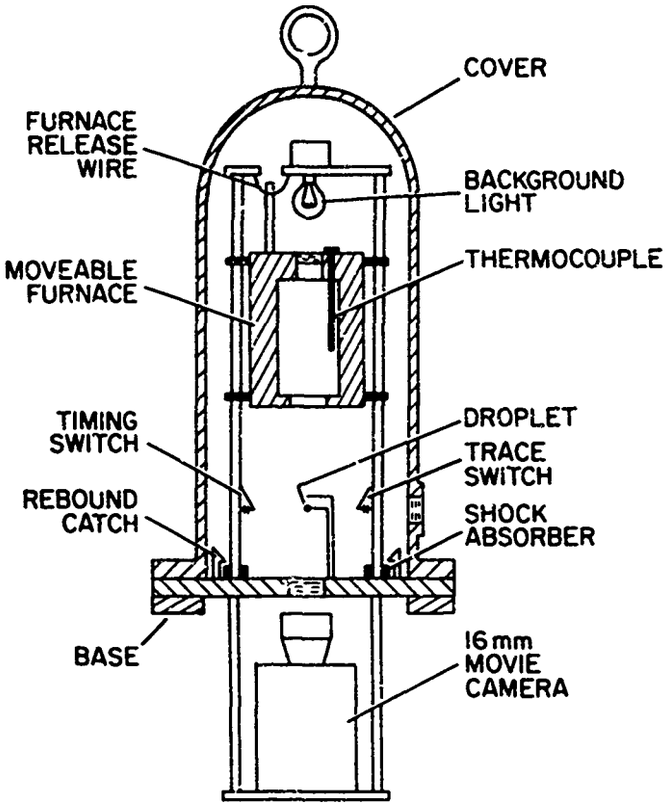

Figure 2.2 Internal Apparatus

it to break. When in the top position, electrical contact was made with the furnace heater circuit. The heater power was controlled by a 120-volt A.C. source through a variac. A chromel-alumel thermocouple was mounted in the furnace at the droplet height. The output of this thermocouple was taken as the test gas temperature. The dimensions of the furnace were 3-1/2 inches O.D. by 2 inches I.D. and 6-1/2 inches in height. The top of the furnace was fitted with a one-inch diameter quartz window which permitted the passage of the background illumination for the camera. The temperature range was room temperature to 1800°F.

The lower chamber was made of an aluminum plate on which several components were mounted. Two pieces of Resilite, 1-1/2 inches high by one inch square, were used to absorb the energy of the falling furnace. At the bottom location, the furnace was latched in place to prevent rebound. Another Westinghouse W-47 lamp was mounted on the plate to provide foreground illumination. Two switches were closed when the furnace was at droplet height, one completing the mount thermocouple circuits and the other completing the internal timing marker circuit for the camera in order to allow synchronization of these records. The mount consisted of two chromel-alumel thermocouples varying from 0.001 to 0.003 inches in diameter. The thermocouple wires were passed through a section of ceramic tubing and on to a terminal board. The thermocouple signals were fed to a CEC 1-165 D.C. amplifier which permitted a gain

up to 1K. The amplifier output was then recorded on a CEC 5-124 18-channel oscillograph using Dataflash 55 oscillograph recording paper. The system was calibrated at about 212°F by a chromel-alumel thermocouple placed in a boiling water bath monitored by a mercury-in-glass thermometer. The furnace temperature was monitored by a Leeds and Northrup millivolt potentiometer and was used as the high temperature calibration for the recorder, the furnace temperature being periodically checked with a mercury-in-glass thermometer at lower temperatures.

2.2 Experimental Procedures

The test procedure can be divided into the preliminary steps and the immediate steps. The preliminary steps consisted of measuring and recording the ambient pressure and temperature, preparing the fuel sample, completing the A.C. power circuits, and turning on the boiling water calibration system. In addition, the camera was loaded with film and the pressure regulator on the high pressure gas bottles was adjusted. The test gas was commercially pure nitrogen. To conduct a test, the furnace was raised and held in position by the release wire. The heater variac was adjusted and the furnace temperature was permitted to stabilize.

Immediately prior to a test, the cover was lowered and secured. The air in the test chamber was evacuated using a Model 1402 Welch vacuum pump. The chamber was filled with nitrogen to

slightly above atmospheric pressure. Then the access plug was removed, permitting nitrogen to flood out the opening while the drop was mounted. The next step was to install the access plug and pressurize the chamber. The test pressure for the high pressure tests was measured on an Acco Helicoid pressure gage with 20 psi subdivisions, while at lower pressures, a Bronze tube Dursgage with 2 psi subdivisions was used. The gages were calibrated using the dead weight test process. After pressurization, the furnace temperature was checked and the droplet was visually inspected through the port window.

If all test conditions were met, the remote control switch was closed. This switch simultaneously started the oscillograph recorder, started the camera and completed the furnace release circuit. The furnace would fall after the release wire was broken and a few seconds were allowed before stopping the test. Then the chamber was depressurized and the cover was unbolted and raised by the hand winch. The furnace was unlatched and raised in preparation for the next test.

2.3 Experimental Data

The raw data from this apparatus consisted of exposed movie film and latensified oscillograph recording paper. The film used was Kodak tri-x negative-emulsion TNX430. The film was processed by using a rewind tank and a portable cloth darkroom. The steps

were first to pass the film through Kodak DK-60A developer, then through Kodak Indicator Stop Bath, then through FR Pro-Fixol Super Concentrated Universal High Speed Fixer - No. 5 size, and finally in a running water bath. The developed film appeared as shown in Figure 2.3. The timing marks were counted and converted into actual time, each timing mark being 1/120-second apart. The marks appeared on the film five frames behind the picture due to the location of the timing light in the camera; therefore, this had to be considered. For calibration purposes, a section of known diameter wire was placed at the droplet position and recorded for a few frames.

The next step in reducing the film data was to project the film frame by frame on a small screen. The projector position was adjusted to provide an enlargement of ten times the drop size. Since the droplet appeared as an ellipsoid, Figure 2.3, the minor and major axes were measured and the measurements were converted to an equivalent spherical diameter. This procedure has been followed by many workers[3,4,5,12,14] in droplet studies. The conversion can be made by basing the equivalent sphere on either an equal volume or an equal surface area sphere. Based on equivalent surface area, the relation is:

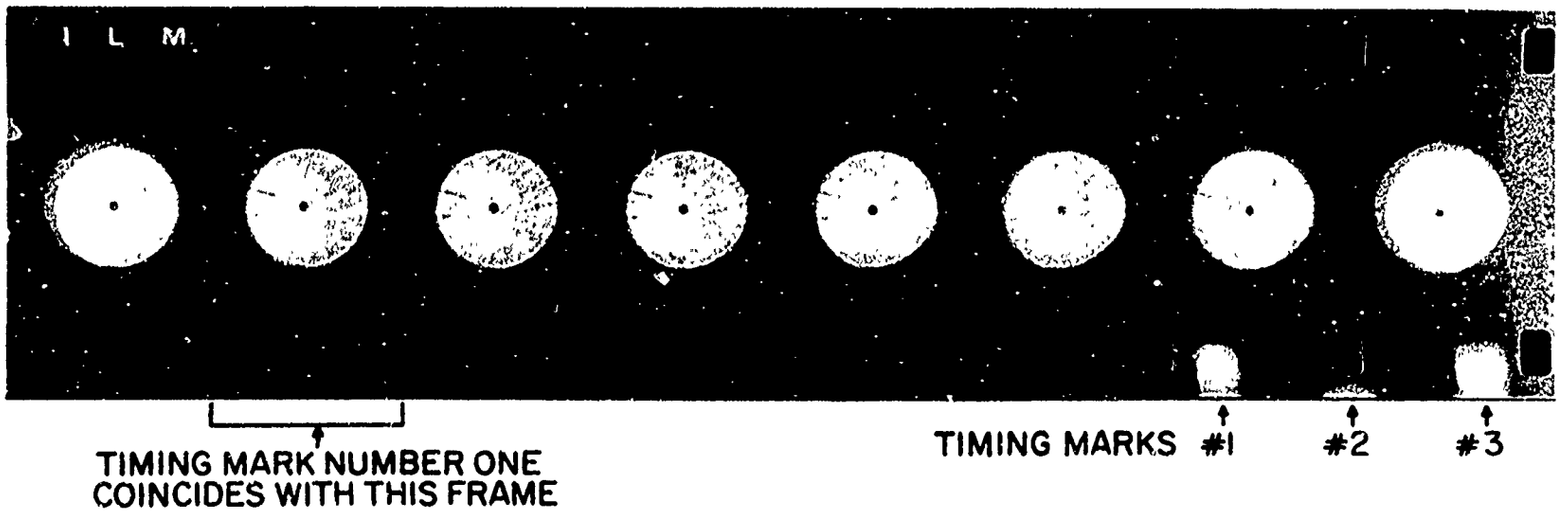

Figure 2.3 Sample Test Film

$$d = \ell_2 \sqrt{\frac{1}{2}\left[1 + \frac{(\ell_1/\ell_2)^2}{\sqrt{(\ell_1/\ell_2)^2 - 1}} \sin^{-1} \frac{\sqrt{(\ell_1/\ell_2)^2 - 1}}{(\ell_1/\ell_2)}\right]} \quad , \tag{2.1}$$

while, based on equivalent volume, the relation is:

$$d = \sqrt[3]{(\ell_1 \ell_2)^2} \quad . \tag{2.2}$$

The difference between the diameter predicted by Equation (2.1) and Equation (2.2) has been demonstrated[3] to be less than 1.5 percent, so Equation (2.2) was chosen because of its simplicity.

The temperature records were marked before the test with the furnace temperature and the 212°F boiling water calibration. The records were then labeled in detail with a temperature scale and a timing scale. The oscillograph recorder was equipped with a timing mechanism which would strike a line normal to the paper axis at 0.1-second intervals. Also, the two traces were distinguished as to liquid and gas phase trace and were appropriately lettered. Since the recording paper was sensitive to ultra-violet radiation, the trace would eventually disappear upon continued exposure to light. Hence, the records were stabilized by spraying each one with Kodak Linograph Stabilizing Lacquer.

CHAPTER III

IGNITION

3.1 Preliminary Experimental Results

Typical experimental results are shown in Figures 3.1 to 3.3. Figure 3.1 is a plot at low pressure of droplet diameter, liquid temperature and gas phase temperature (as sensed by the thermocouple located in the boundary layer about 1/16-inch above the droplet). The independent variable is time. Figure 3.2 is a similar plot for a high pressure test. The fuel employed for this data was ethyl nitrate.

Several comparisons can be made from these figures. First, at low pressure, Figure 3.1, the droplet lifetime is considerably longer than at high pressure, Figure 3.2. At low pressure, the liquid temperature had an inflection at roughly the same time as the diameter begins to decrease. However, at high pressure, no liquid temperature inflection is observed. At low pressure, a wet bulb temperature is reached as indicated by the nearly steady liquid temperature. This occurs during the period where the bulk of the evaporation occurs. At high pressures, the liquid temperature is seen to rise throughout the droplet lifetime. Also,

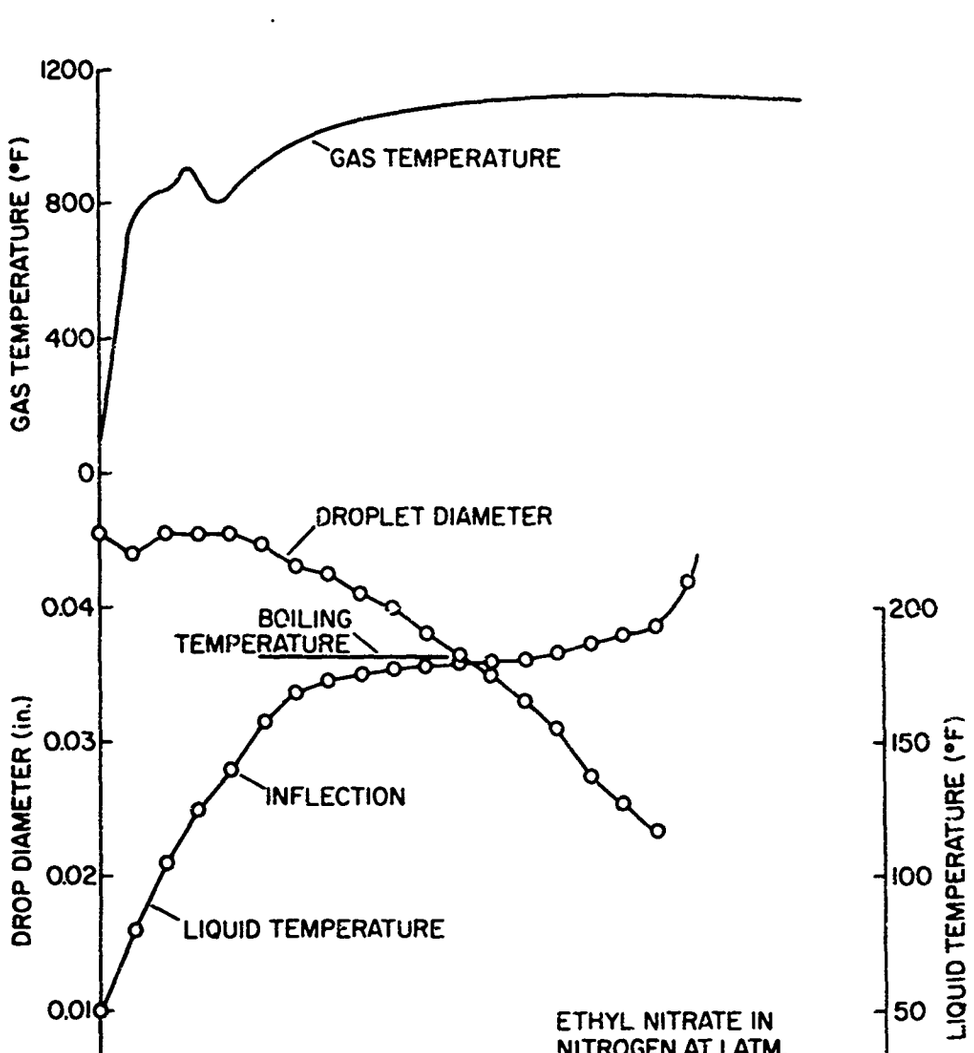

Figure 3.1 Low Pressure Results

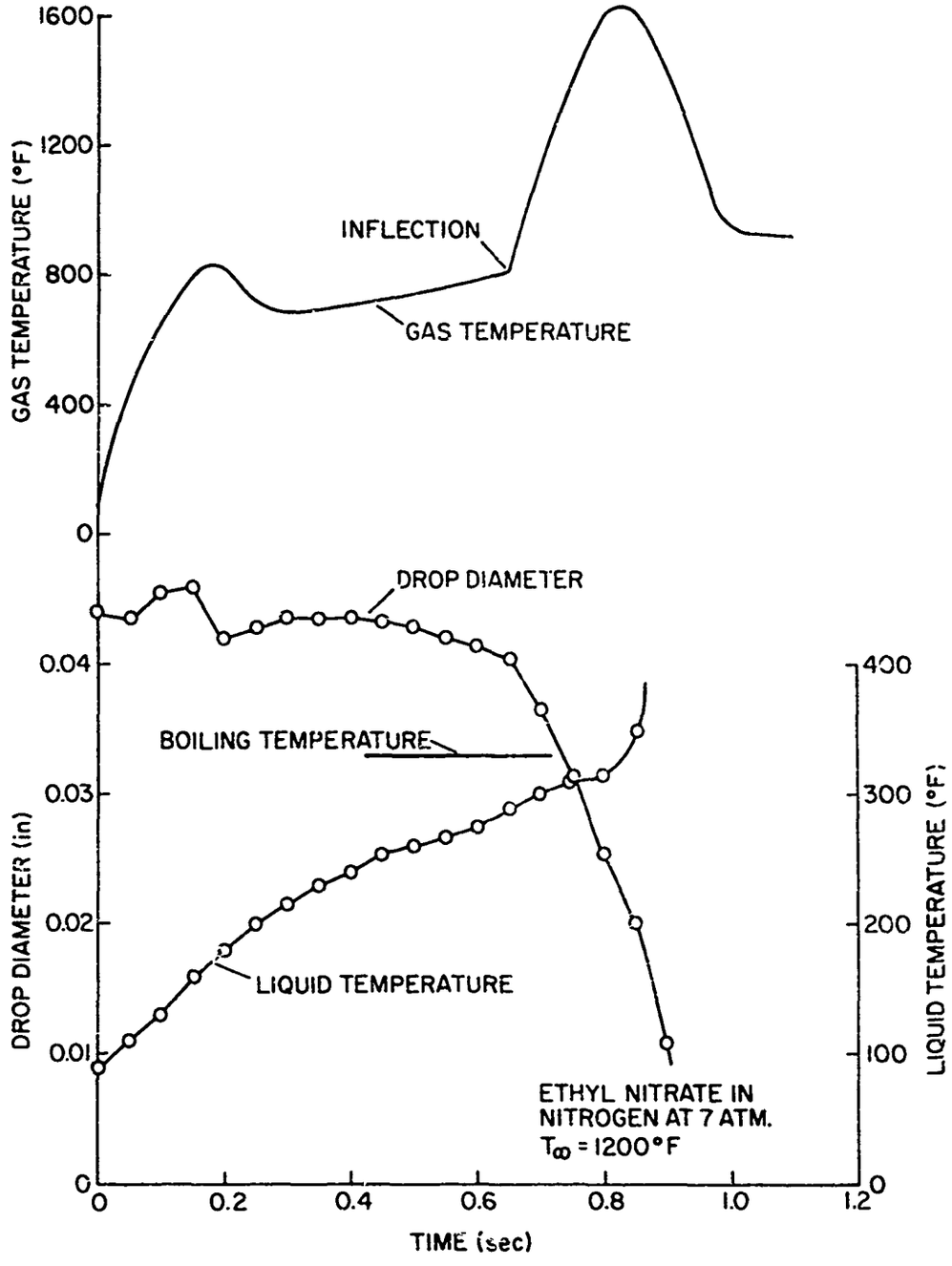

Figure 3.2 High Pressure Results

at high pressures, there is a clearly observable gas phase temperature inflection roughly coinciding with the time that the drop diameter begins to decrease.

The fluctuation of the diameter record at the very beginning is believed to be due to apparatus vibrations caused by the furnace as it strikes the resilite pads. The droplet was observed to oscillate briefly on the probe during this period.

The rapidity of the decomposition process at high pressures is indicated more clearly in Figure 3.3. This is a plot of the droplet diameter squared versus time. Taken literally, the radius regression rate is the rate at which the drop radius decreases with time. The rapid change in radius regression rate with pressure as seen in Figure 3.3 is characteristic of monopropellants. That is, the rate would not change as rapidly with pressure for a bipropellant.

Several workers[5,13,14,15] have shown that the liquid temperature approaches, quite closely, the boiling temperature when the droplet is at its wet bulb state. Figures 3.4 and 3.5 show a comparison between the boiling temperature and the maximum measured liquid temperature at various pressures for the four fuels tested. The PGDN data was taken from Reference 14. At low pressures, the measured liquid temperatures are closely approximated by the boiling temperature. However, at high

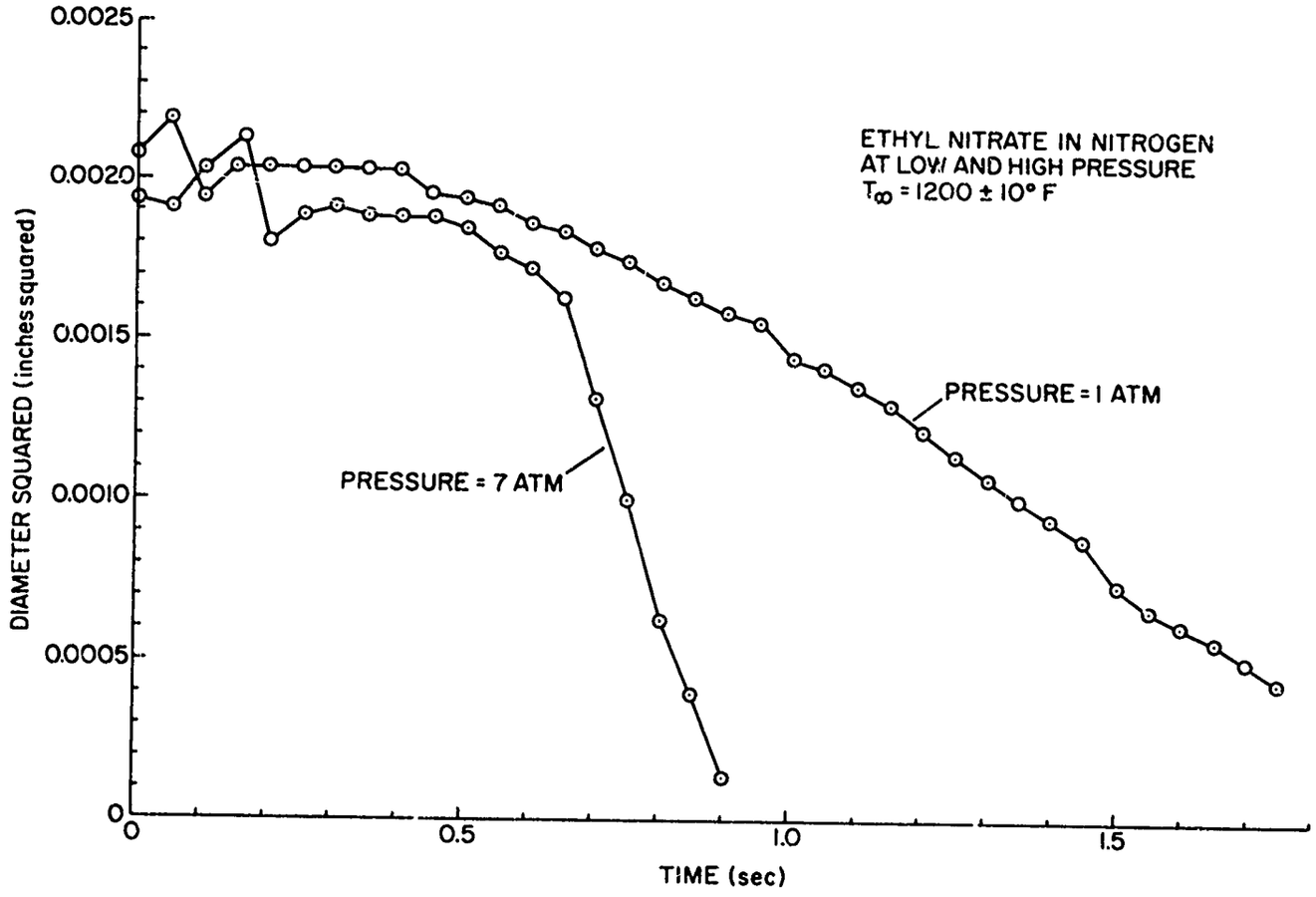

Figure 3.3 Diameter Squared Results

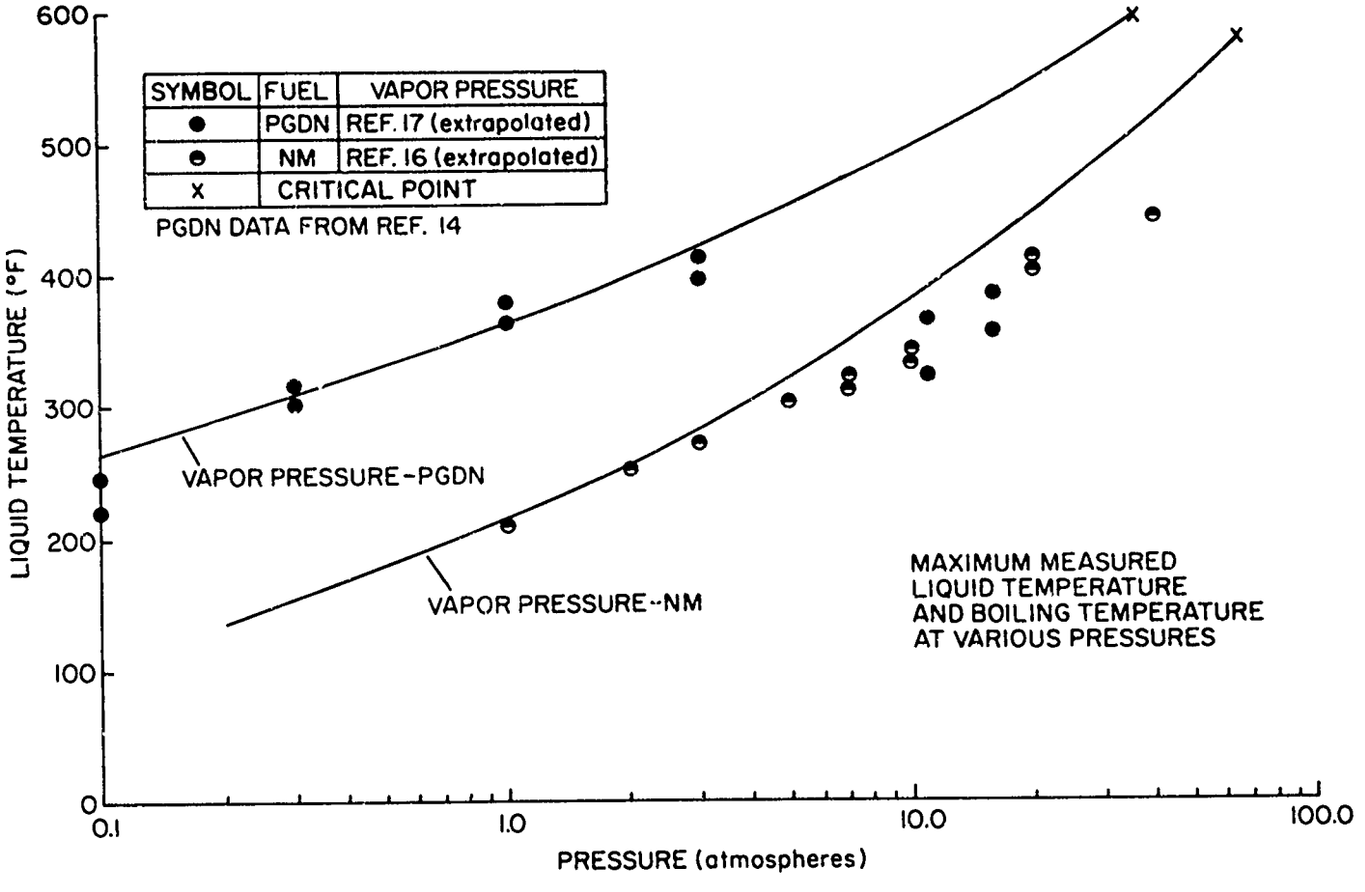

Figure 3.4 Liquid Temperature at Various Pressures PGDN and NM

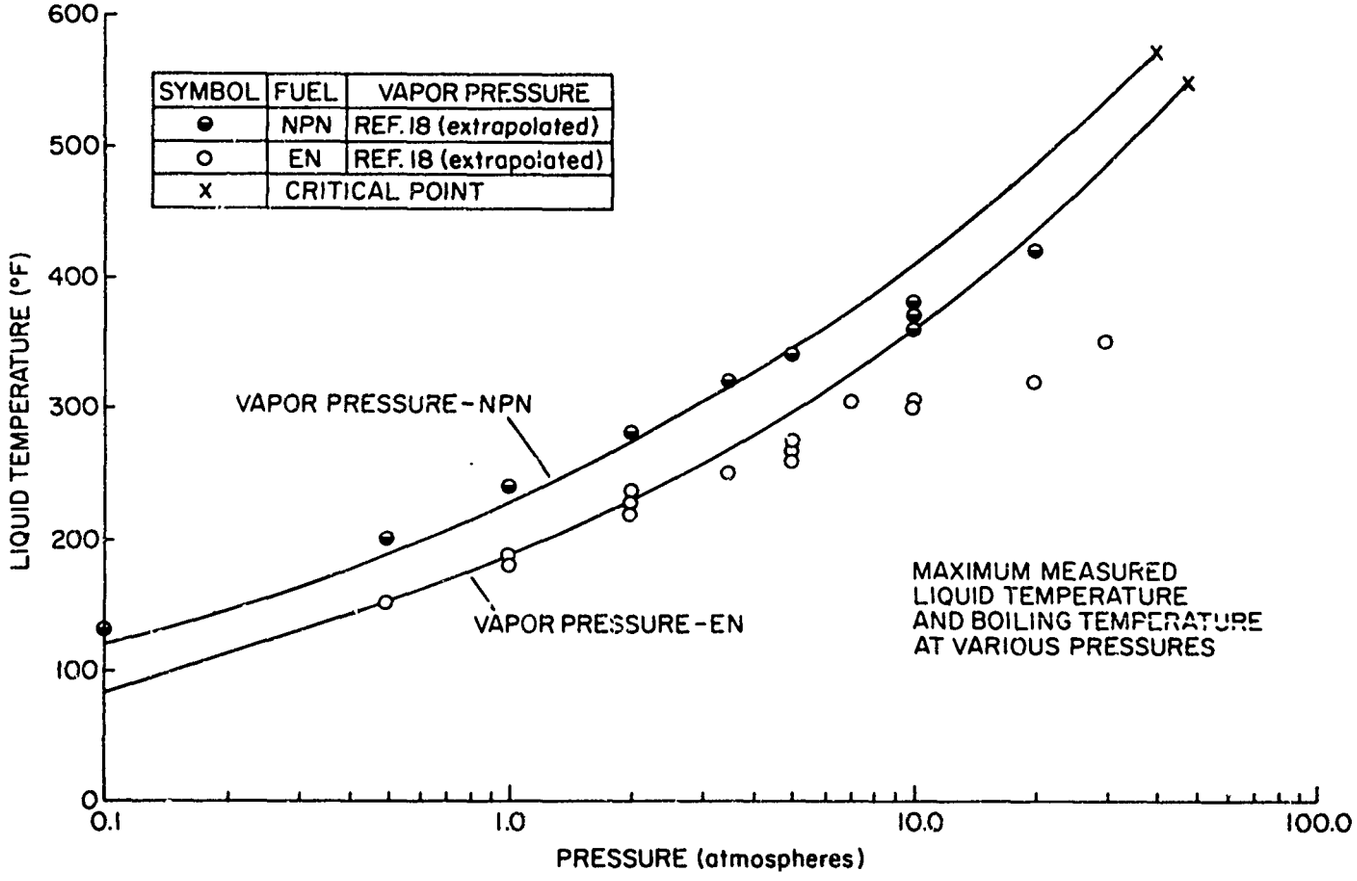

Figure 3.5 Liquid Temperature at Various Pressures NPN and EN

pressures, the maximum liquid temperature lies significantly below the boiling temperature, particularly for PGDN and EN.

3.2 Ignition Model

From Figure 3.1, it is observed that the liquid temperature inflection occurs at about the same time that the drop diameter begins to decrease. This is also at about the same time that the liquid temperature begins to reach a constant value near the boiling temperature. From Figure 3.2, the gas temperature inflection and diameter decrease occurs at about the same time that the liquid temperature reaches a value near the boiling temperature. If the time at which the inflections occur is defined as the ignition time, it appears reasonable to take the time for the droplet to heat up to the boiling temperature as a first estimation of ignition time, the justification being that these events occur at about the same time. If evaporation is neglected, the calculation of the heat-up time would be analogous to determining the time required for a steel ball initially at T_o to reach a temperature T after being immersed in a hot bath at T_∞.

The heat-up model developed by Karhan[14] followed this line of reasoning and, hence, was employed to estimate ignition times. Karhan developed two theoretical models. His assumptions were:

1) The droplet is composed of a single chemical species.

2) In the first model, the droplet temperature is assumed uniform throughout the droplet, but varying with time. The second model considers transient temperature gradients in the droplet.

3) Properties are constant in both the liquid and gas phases.

4) No surface evaporation occurs and the droplet radius remains constant.

5) The heat transfer and diffusion processes are spherically symmetrical.

6) The influence of the mass transfer on the heat transfer characteristics of the boundary layer around the droplet is neglected.

7) The time required for the droplet to heat up to the boiling point is an estimation of ignition time.

Karhan showed the difference between the ignition time predicted by the two models to be small and, hence, the infinite conductivity model was employed due to its simplicity. The energy equation can be written as:

$$S\ B\ A_R\ (T_\infty^4 - T^4) + h_c\ A_R\ (T_\infty - T) = \rho\ C_p\ V \frac{dT}{dt} \quad . \quad (3.1)$$

Hottel, et al[2], have shown that B should be about 0.5 for hydrocarbon fuels in the diameter range of the present experiment. In addition, Faeth[5] experimentally measured B and found the value

to be 0.44 for iso-octane. He found no detectable variation of this value over a drop diameter range of 0.025 to 0.045 inches and furnace temperatures of 1000° to 1500°F. Thus, a value of 0.5 as determined from Reference 2 was used. Other properties employed in the calculations may be found in Appendix B.

Assuming $T_\infty^4 \gg T^4$, Equation (3.1) may be readily integrated to yield:

$$t = \frac{\rho_\ell C_p d^2}{6 \, Nu \, K_g} \ell_n \left[\frac{1 + \frac{Nu \, K_g}{S \, Bd_o \, T_\infty^4} (T_\infty - T_o)}{1 + \frac{Nu \, K_g}{S \, Bd \, T_\infty^4} (T_\infty - T_s)} \right] . \qquad (3.2)$$

3.3 Ignition Results

Equation (3.2) permits one to calculate the time t for the liquid to reach any temperature T_s. This equation was then employed to predict the time for the liquid to reach various temperatures and a comparison was made with measured liquid temperatures. Figure 3.6 is a plot of liquid temperature as a function of time for typical low and high pressure tests. At both low and high pressure, the theoretical and experimental results agree reasonably well during the early part of the heat-up process. However, discrepancies appear as the liquid approaches its boiling temperature with the predicted temperature being greater than the measured value. This is undoubtedly due to neglecting evaporation

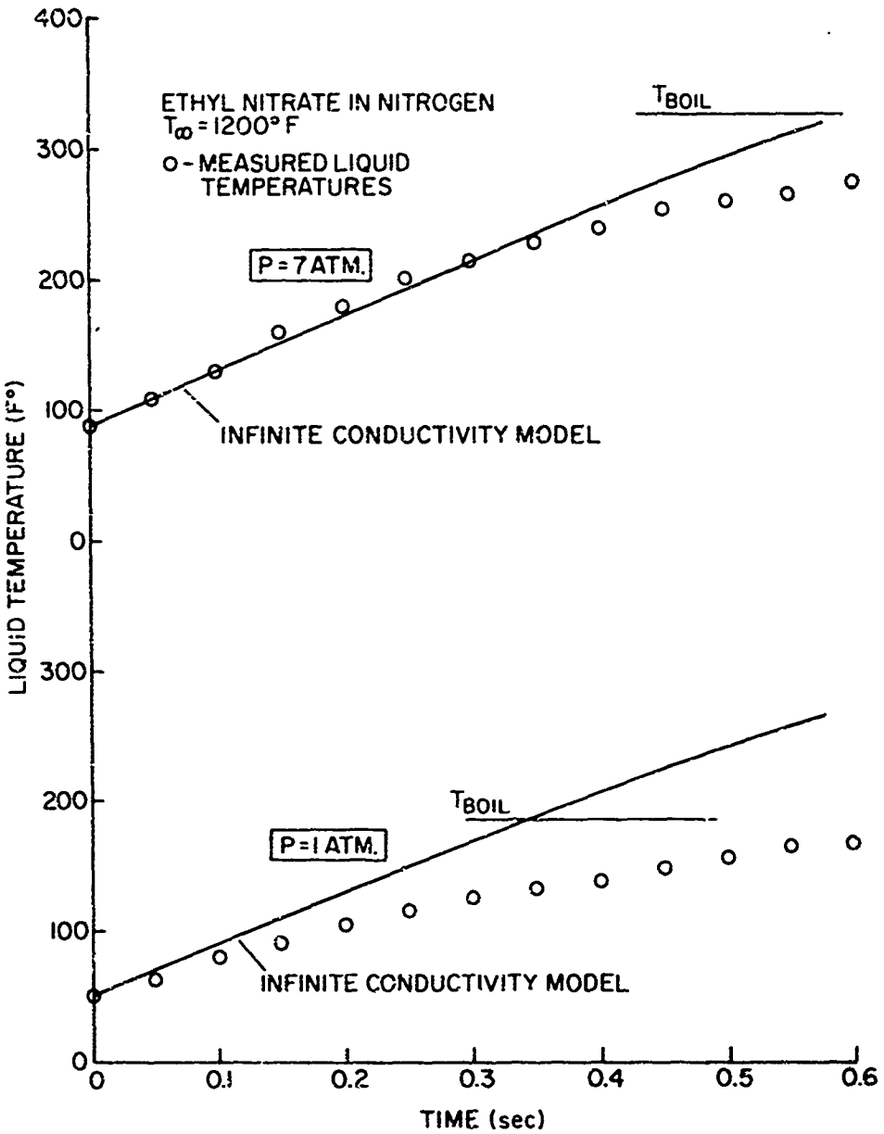

Figure 3.6 Measured and Predicted Liquid Temperature

in the heat-up model. Since the ignition time is the time for the model to predict the boiling temperature, the results at low pressure for time greater than 0.35 seconds can be disregarded. Hence, over the range of temperatures considered relevant, the model does agree within reason with the measured results.

Equation (3.2) was then employed to calculate the time for the liquid to heat up to the boiling temperature. Figure 3.7 shows the variation with diameter of the predicted and measured ignition time for EN. The measured ignition time follows the trend of the predicted results, but appears to be consistently greater over the diameter range. An explanation of this consistent discrepancy will be given later.

Figure 3.8 shows the ignition time variation with pressure and temperature for ethyl nitrate in nitrogen. At low pressures, the liquid temperature inflection and major diameter decrease (or diameter break) were used as an indication of ignition. At high pressures, the gas temperature inflection and diameter break were taken as the indication of ignition. The measured times follow the trend of the predicted values at low pressure, but are considerably lower at high pressure. The dashed curve shows the time for the liquid to reach 355^{o}F which is the maximum measured liquid temperature over the test range for EN, Figure 3.5.

Figure 3.9, taken from Reference 14, shows a similar plot for PGDN. Again, the measured times follow the trend of the

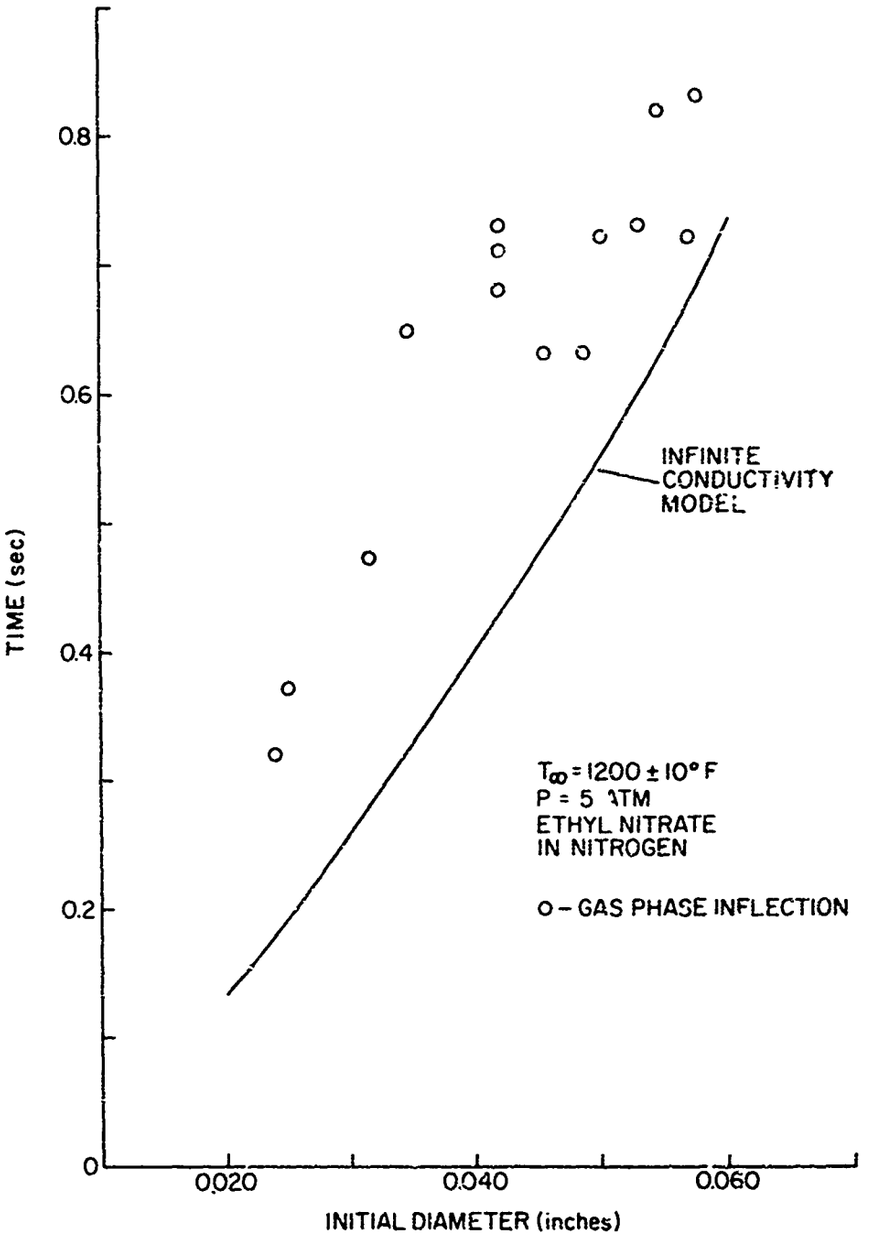

Figure 3.7 Ignition Time Versus Initial Diameter

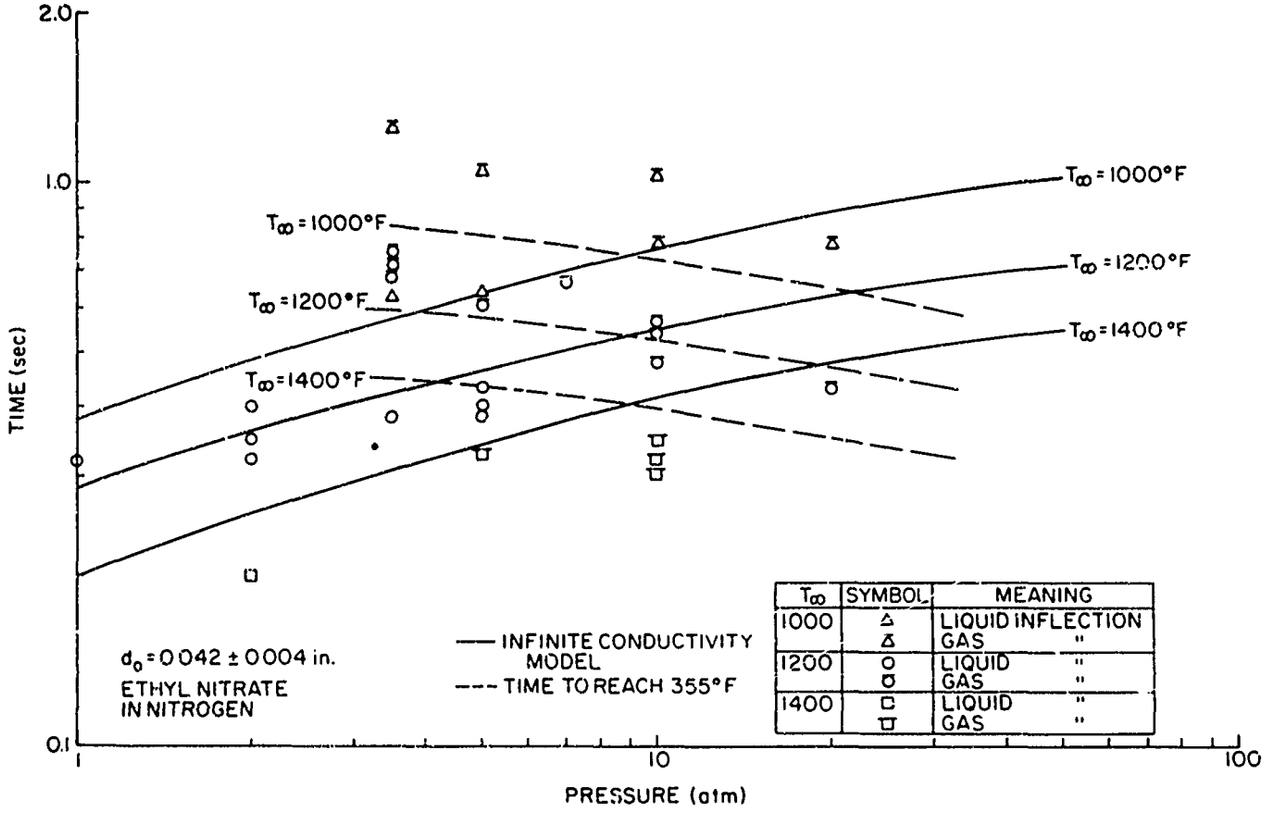

Figure 3.8 Ignition Time Versus Pressure for EN

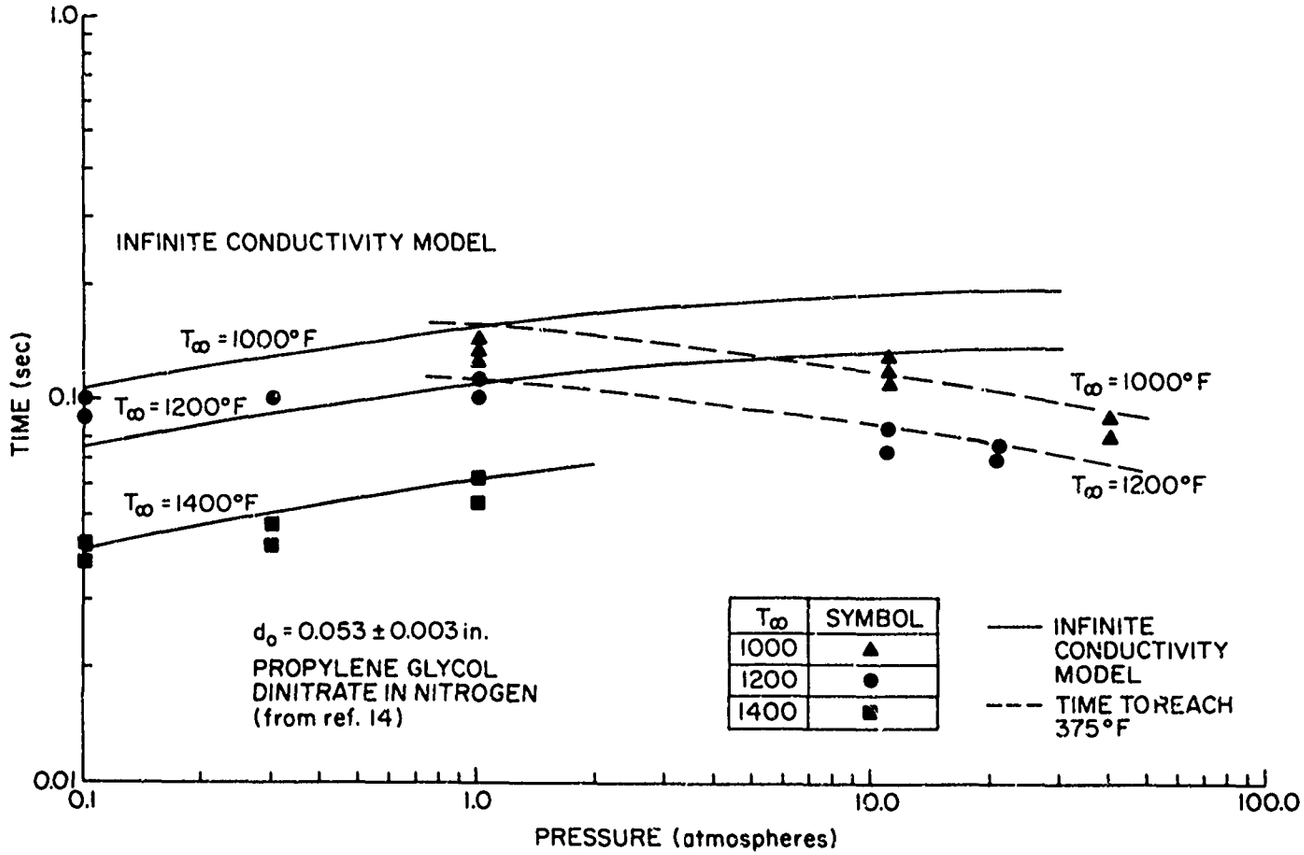

Figure 3.9 Ignition Time Versus Pressure for PGDN

heat-up model at low pressure but fall considerably lower at high pressure. The dashed curve is the time for the liquid to reach 375°F at various pressures. The value of 375°F roughly corresponds to the average of maximum measured liquid temperatures in the high pressure regime of Figure 3.4.

Figure 3.10 shows the ignition time variation with pressure for nitromethane. The criterion for ignition was chosen as diameter break since the temperature inflections for nitromethane were very slight and, hence, difficult to interpret. Once again, the low pressure measurements follow the trend of the heat-up model but are shorter in the high pressure regime. The second set of points on Figure 3.10 shows the time for the liquid to reach 95 percent of the measured steady state temperature. These points follow the trend of the heat-up model but, of course, are much larger. Since these points follow the trend at low pressure, one could infer some relation between the maximum liquid temperature and the occurrence of the ignition event.

On all three Figures, 3.8, 3.9 and 3.10, the ignition event follows quite closely the heat-up model at low pressure. But the heat-up model is related to the maximum liquid temperature. Therefore, it appears that the ignition event is related closely to the maximum liquid temperature at low pressure. In addition the 95 percent points on Figure 3.10 follow the trend of the heat-up model at low pressure, further strengthening this argument.

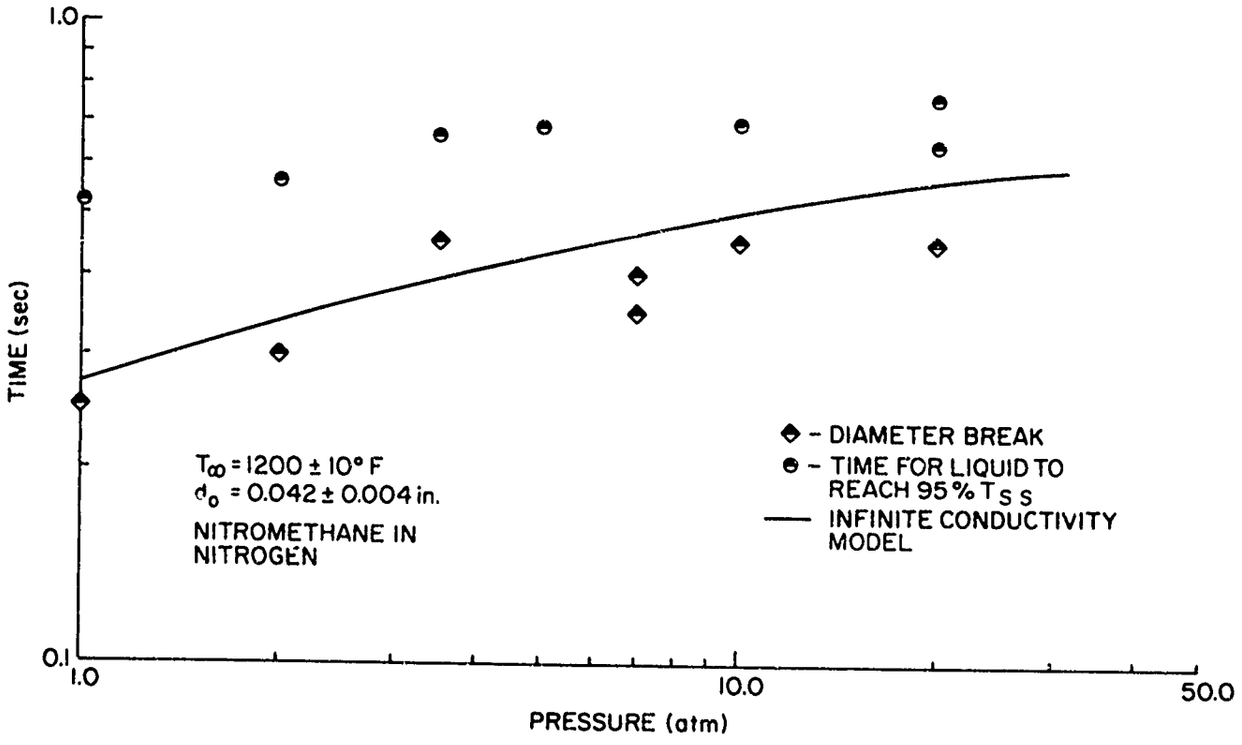

Figure 3.10 Ignition Time Versus Pressure for NM

In the high pressure regime, the ignition does not follow the heat-up model. Rather, ignition seems to follow the time predicted to reach a temperature equal to some constant liquid temperature. Hence, ignition appears to be related to liquid temperature--a maximum liquid temperature in the low pressure regime and a constant liquid temperature in the high pressure regime.

Before proceeding, we must examine the definition of ignition. In the general sense, ignition means the point at which chemical reaction becomes apparent. If a droplet were exposed to room temperature at atmospheric pressure, chemical reaction would be so slow as to be undetectable. Under these conditions, ignition is meaningless. The liquid would vaporize and diffuse to the surroundings. At elevated pressure and temperature, however, the reaction proceeds much faster and the point in time that reaction begins is the ignition point. The reaction must take place in either the liquid or the vaporized fuel surrounding the droplet since combustible material is present only there.

Gas phase studies[7,8,10,11,19] have shown the reaction for the fuels employed to be first-order. Phillips[19] has shown that there is no appreciable difference in the reaction rates between the liquid and gas phase reactions. The reciprocal of the reaction rate constants may then be taken as a characteristic reaction time for the liquid and gas phases. Figure 3.11 shows the effect of temperature on the characteristic time for the fuels studied.

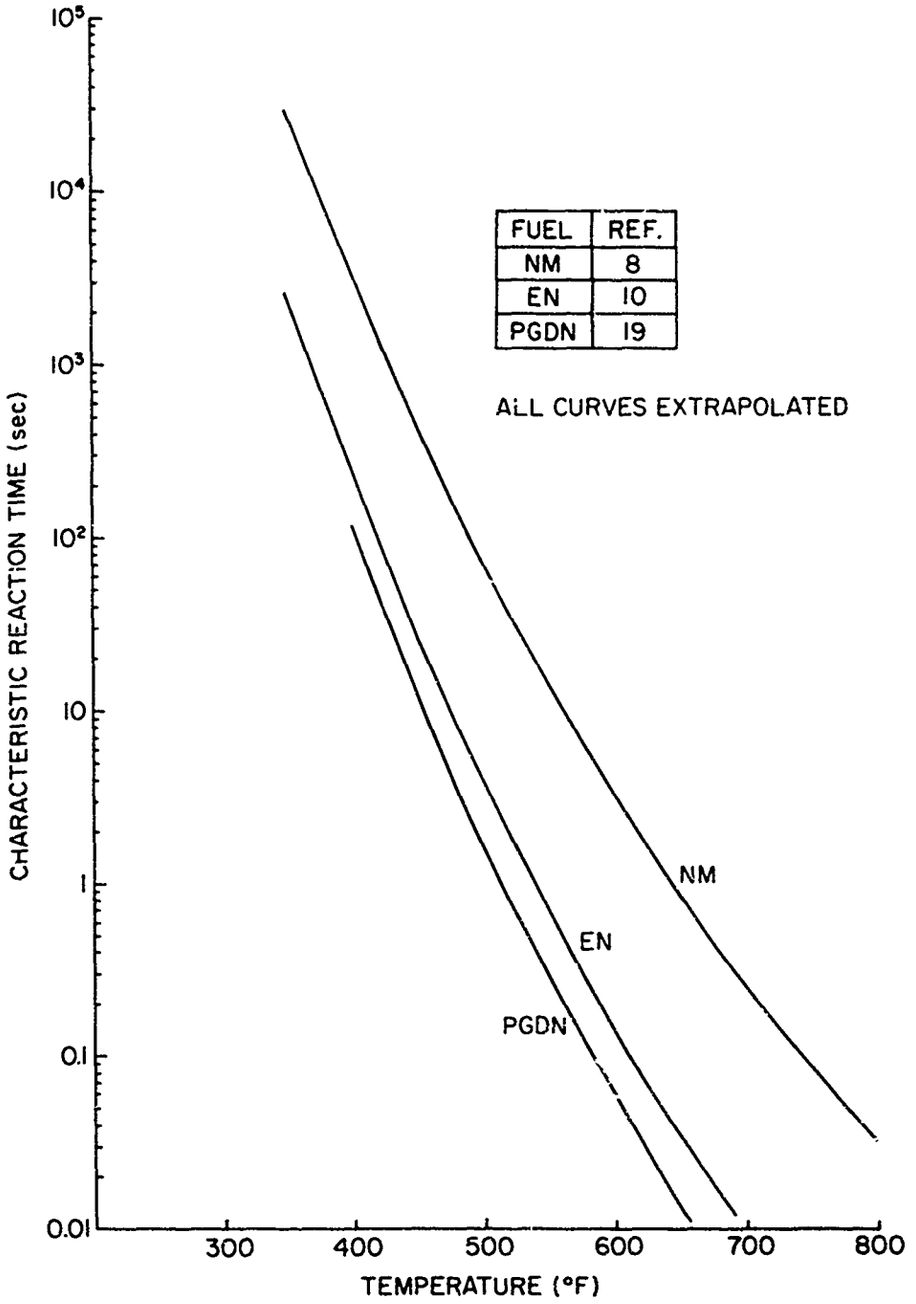

Figure 3.11 Characteristic Reaction Times

It was shown that the reaction must occur in either the liquid or gas phase, but the maximum measured liquid temperature in all cases was about $440^{o}F$ or smaller, Figures 3.1 and 3.2 . At these temperatures, the reaction times from Figure 3.11 is always greater than 10 seconds. Since the ignition times measured were of the order of one second, we must exclude liquid phase reactions as a possible ignition mechanism over this test range.

The equation for the conservation of energy for a motionless droplet may be written in dimensionless form in the following way:

$$\frac{1}{\eta^2}\frac{d}{d\eta}\left(\eta^2 \nu\theta - \eta^2 \frac{d\theta}{d\eta}\right) = \frac{d^2 A\Delta H_R P Y_{fo}}{4 K_g T_\infty} \exp\left(-\frac{\theta_R}{\theta}\right) . \quad (3.3)$$

The term on the right side carries the effect of chemical reaction, the effect being large when the term is large. This term has the product PY_{fo} which is proportional to the vapor pressure of the liquid. The vapor pressure of the liquid, however, is a strong function of liquid temperature. Hence, through the term on the right side of Equation (3.3), the liquid temperature exerts a strong effect on the chemical reaction occurring in the gas phase. At high pressure, the sequence of events is as follows:

1) The droplet begins to heat up when immersed in the hot gas.

2) Before the liquid temperature reaches the boiling temperature, the term on the right side of Equation (3.3) reaches a sufficiently large value for the chemical reaction to begin in the gas phase.

3) This disturbance is detected by the gas phase thermocouple indicating the ignition event.

As the pressure varies in the high pressure regime, the same sequence will be followed with the ignition event always occurring before the liquid temperature reaches the boiling temperature. Thus, the dashed lines in Figures 3.8 and 3.9 give a good correlation of ignition. These lines were plotted for a constant temperature which shall be defined as the "ignition temperature."

The test conditions for the data of Figure 3.7 were at a temperature of 1200°F and a pressure of 5 atmospheres. A close inspection of Figure 3.8 shows that at these conditions the ignition time predicted by the ignition temperature concept are about 25 percent longer than the ignition time predicted by the heat-up model. In addition, the gas phase inflections follow the dashed curve. Figure 3.7, however, shows a comparison of ignition times as predicted by the heat-up model to the ignition time as determined by the gas phase inflection. The gas phase inflections on this curve are also about 25 percent above the heat-up model predictions. Thus, the consistent discrepancy noted in Figure 3.7

is reasonable since the heat-up model predicts ignition times lower than the gas phase inflections for these test conditions.

The ignition temperature concept appears to give a reasonable explanation for the occurrence of ignition for the high pressure regime only in the test range encountered. The applicability o. this concept to other conditions is unknown since the drop diameter and free stream temperature also appear in Equation (3.3). A more complete investigation is necessary before any general conclusions can be made.

CHAPTER IV

COMBUSTION

4.1 Combustion Model

A bipropellant system is characterized by a fuel droplet burning in an oxidizing atmosphere. In this case, the flame surrounding the droplet is a diffusion flame. The flame position in the boundary layer is governed by the stoichiometry of the flame and by the diffusion characteristics of the gases. Therefore, for bipropellants, a good estimate of the burning rate can be made with little consideration of the chemical kinetics of the combustion process.

The situation is quite different for monopropellants. The propellant evaporates at the drop surface and flows toward the flame zone as a premixed combustible material. Therefore, for monopropellants, the flame positions itself so that its rate of propagation toward the droplet through the combustible material is just balanced by the outward propellant flow. Since the propagation rate of the flame is controlled very strongly by reaction rates in the flame zone, the position of the flame in the boundary layer and, in turn, the burning rate of the droplet is strongly influenced by chemical kinetics.

An a priori calculation of droplet burning rates may be attempted since there is sufficient information in the literature on the chemical kinetics of some of the fuels tested. However, a different approach was employed here to study the combustion process. The procedure consisted of utilizing measured burning rates, within a simplified model of the combustion process, to infer kinetic parameters for comparison with the values reported in the literature. The primary advantage of this procedure is that it greatly simplified the numerical computations.

The theoretical approach follows a method first developed by Spalding[21] for adiabatic burning (the case where the temperature of the gas surrounding the flame is equal to the flame temperature) and later modified by Williams[15] to consider nonadiabatic burning. As formulated, this model does not account for the influence of convection on the combustion process.

Employing Williams' formulation, Karhan[14] found that abnormally large values of thermal conductivity for the gas phase were needed in order to obtain activation energies in reasonable agreement with the values reported in the literature. He suggested that the apparently excessive heat loss from the nonadiabatic flame may be due to natural convection. As a further confirmation of this suggestion, Faeth[9] has shown that the nonadiabatic flame is particularly vulnerable to forced convection. Thus, in the present work, Williams' analysis is modified to account for the effect

of natural convection and the resulting formulation is employed to correlate the measured burning rate results.

The combustion model considered in the analysis is shown in Figure 4.1. It is assumed that the droplet is concentrically surrounded by an infinitely thin spherical flame. Natural convection is treated by way of the familiar film theory approximation. In this theory, the actual convective flow field is replaced by a field with no convection but with a constant outer radius r_∞, where the gas temperature is specified to be equal to the free stream temperature. For nonadiabatic systems, the radius r_∞ is selected so that the overall heat and mass transfer characteristics of the stagnant film are equivalent to empirical measurements of transport rates in the actual system. The only consideration of the flamelike structure in the boundary layer in the present study was to redefine the Grashof number in the empirical heat transfer correlation in a way more appropriate to flames as suggested by Spalding.[30]

Other assumptions employed in the model are as follows:

1) The droplet is at its equilibrium or "wet bulb" state and the droplet temperature is assumed to be constant and equal to its boiling temperature at the total pressure of the test.
2) Quasi-steady burning is assumed.
3) All gases obey the ideal gas law.

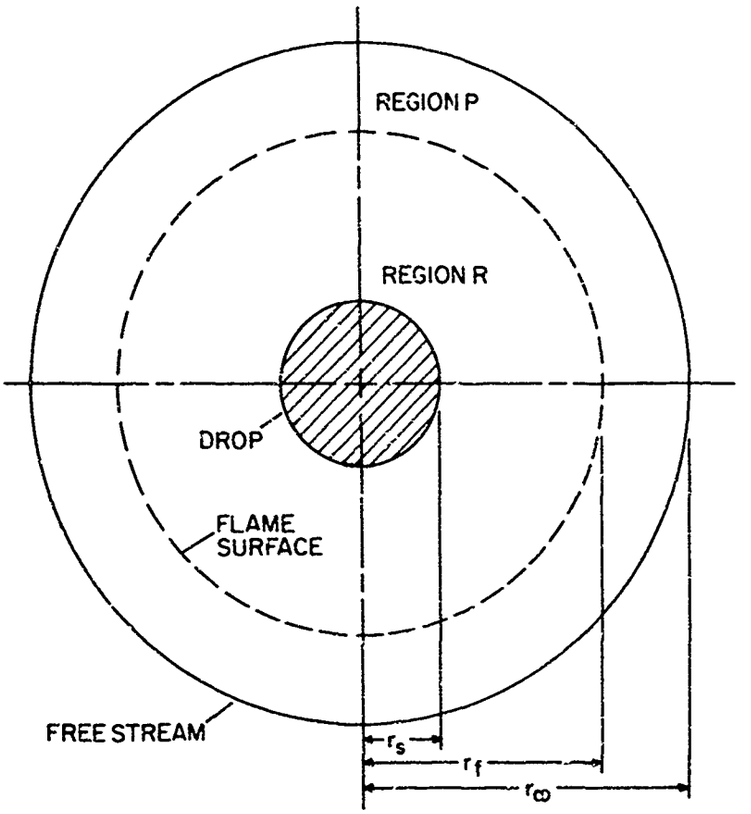

Figure 4.1 Combustion Model

4) The total pressure is constant.

5) All liquid properities are constant.

6) All gas phase properties are constant and equal to those for nitrogen gas, with one exception being the specific heat at constant pressure. The determination of the specific heat was based on the diffusing material and will be discussed later.

7) At the flame, a one-step reaction is assumed.

8) An effective heat of reaction is used that is based on conservation of energy during adiabatic burning, with due allowance for dissociation.

9) The Lewis number is unity.

10) Radiation heat transfer to the droplet is neglected.

The last assumption seems justified since separate calculations showed that of the heat transferred to the droplet, a maximum of 14 percent was due to radiation from the high temperature furnace wall. This assumption greatly simplifies the numerical computations.

Conservation of mass as applied to a control volume bounded by spheres of radius r and $r + dr$ is:

$$\frac{d}{dr} (r^2 \dot{m}'') = 0 \quad . \qquad (4.1)$$

This equation may be readily integrated to produce the following result:

$$r^2 \dot{m}'' = \text{constant} \quad . \tag{4.2}$$

The steady flow energy equation for a similar control volume is:

$$r^2 \dot{m}'' C_p \frac{dT}{dr} - \frac{d}{dr}\left(r^2 K \frac{dT}{dr}\right) = 0 \quad , \tag{4.3}$$

with the boundary conditions:

$$\begin{aligned} &\text{at } r = r_s \ , \ T = T_s \\ &\text{at } r = r_f \ , \ T = T_f \\ &\text{at } r = r_\infty \ , \ T = T_\infty \quad . \end{aligned} \tag{4.4}$$

Equation (4.3) may be integrated as shown in Appendix A to yield the temperature distribution. In region R ,

$$T = \frac{T_f \exp(-a/r_s) - T_s \exp(-a/r_f) + (T_s - T_f) \exp(-a/r)}{\exp(-a/r_s) - \exp(-a/r_f)} \quad . \tag{4.5}$$

Similarly, for region P , the result is:

$$T = \frac{T_\infty \exp(-a/r_f) - T_f \exp(-a/r_\infty) + (T_f - T_\infty) \exp(-a/r)}{\exp(-a/r_f) - \exp(-a/r_\infty)} \quad . \tag{4.6}$$

Conservation of energy may also be applied at the drop surface and at the flame front to supply two additional relations. At the drop surface,

$$K \frac{dT}{dr}\bigg|_{r_s} = \dot{m}'' \left[h_g (T_s) - h_\ell (T_s) \right] \quad , \qquad (4.7)$$

while at the flame front:

$$- K \frac{dT}{dr}\bigg|_{r_f^-} + \dot{m}_f'' h_R (T_f) = - K \frac{dT}{dr}\bigg|_{r_f^+} + \dot{m}_f'' h_p (T_f) \quad . \qquad (4.8)$$

The solution of Equations (4.7) and (4.8) may be found in Appendix A. In dimensionless form, these solutions may be written as:

$$\sigma_f = a/r_s \left\{ \frac{a}{r_s} + \ell n \left[\frac{1 + \alpha + Q - \theta_s}{Q} \exp \left(\frac{a}{r_s \sigma_\infty} - \frac{a}{r_s} \right) - \frac{\alpha}{Q} \right] \right\} \qquad (4.9)$$

and

$$\theta_f = \theta_s - \alpha - Q + (1 + \alpha + Q - \theta_s) \exp \left[- \frac{a}{r_s} \left(\frac{1}{\sigma_f} - \frac{1}{\sigma_\infty} \right) \right] \quad . \qquad (4.10)$$

In an attempt to estimate the free stream radius r_∞, the film theory correlation was employed. In the absence of chemical reactions, the conservation of energy principle for a stagnant boundary layer is:

$$\frac{d}{dr} \left(r^2 \frac{dT}{dr} \right) = 0 \quad . \qquad (4.11)$$

the boundary conditions are:

$$T = T_s \text{ at } r = r_s \quad ,$$
$$T = T_\infty \text{ at } r = r_\infty \quad . \tag{4.12}$$

Equation (4.11) may be integrated, as shown in Appendix A, to produce the temperature distribution in the film as follows:

$$T = T_s + \frac{T_\infty - T_s}{r_s \left(\frac{1}{r_s} - \frac{1}{r_\infty}\right)} + \frac{T_\infty - T_s}{r \left(\frac{1}{r_\infty} - \frac{1}{r_s}\right)} \quad . \tag{4.13}$$

The heat transferred to the droplet may be expressed by the Fourier conduction law as follows:

$$\dot{q}'' = K \left.\frac{dT}{dr}\right|_{r_s} \quad . \tag{4.14}$$

The same heat flux through the film may also be expressed by Newton's law of cooling as:

$$\dot{q}'' = h_c \left(T_\infty - T_s\right) \quad . \tag{4.15}$$

Evaluating the temperature gradient in Equation (4.14) from Equation (4.13) and equating the conductive and convective heat fluxes results in:

$$\frac{h_c}{K} = 1/r_s^{\,2} \left(\frac{1}{r_s} - \frac{1}{r_\infty}\right) \quad . \tag{4.16}$$

The Nusselt number may be introduced as follows:

$$Nu = \frac{h_c d_s}{K} \quad . \tag{4.17}$$

By substituting Equation (4.16) into Equation (4.17) and introducing a dimensionless radius, the result is:

$$\sigma_\infty = \frac{Nu}{Nu - 2} \quad . \tag{4.18}$$

Thus, Equation (4.18) shows the relation between the free stream radius σ_∞ and the heat transfer characteristics Nu for the film theory approximation.

Ranz and Marshall[26] have shown that the heat transfer characteristics of liquid droplets may be correlated by the following empirical relation:

$$Nu = 2 + 0.6\ Pr^{1/3}\ Gr^{1/4} \quad . \tag{4.19}$$

This equation couples the actual heat transfer rates to the film theory approximation since the Prandtl number and Grashof number were based on actual boundary layer properties. To account for the presence of a flame in the actual boundary layer, the Grashof number was modified to account for the high temperature, low density gas at the flame. The Grashof number may be written as:[29]

$$G_r = \frac{d^3 \rho^2 g}{\mu^2} \left(\frac{\rho_s - \rho_\infty}{\rho_s} \right) \quad . \tag{4.20}$$

As suggested by Spalding,[30] for a burning droplet, the density of the hot gas surrounding the droplet is much smaller than the density at the droplet surface:

$$\rho_\infty \ll \rho_s \quad . \tag{4.21}$$

Thus, Equation (4.20) may be written:

$$G_r = d^3 \rho^2 g / \mu^2 \quad . \tag{4.22}$$

One of the experimental measurements was the slope of the diameter versus time curves. The slope of this curve was proportional to the radius regression rate $\dot{r}$. For quasi-steady burning and constant liquid density, conservation of mass applied to the droplet results in the following:

$$\dot{m} = 4 \rho \pi r_s^2 \dot{r} \quad . \tag{4.23}$$

Hence, Equation (4.23) permits one to calculate the mass flux from known properties and the experimental radius regression rates.

During quasi-steady combustion, the inward propagation rate of the flame is just equal to the outward flow rate of the combustible material. This may be expressed as follows:

$$\rho_f v_f = \dot{m}/(4 \pi r_f^2) = \dot{m}/(4 \pi r_s^2 \sigma_f^2) \quad . \tag{4.24}$$

This relation is needed since, as will be shown later, the solution for the kinetic constants entails the plotting of $\rho_f v_f$ as a function of temperature and pressure.

The next step in the solution of the combustion equations was the evaluation of the properties. The first parameter to be determined was the adiabatic flame temperature. Altmann[25] shows that, at the adiabatic flame temperature, thermodynamic calculations indicate that the equilibrium composition for nitromethane is very closely represented by:

$$CH_3NO_2 = 0.2CO_2 + 0.8CO + 0.8H_2O + 0.7H_2 + 0.5N_2 \quad . \quad (4.25)$$

Separate thermodynamic calculations were made using JANAF Thermochemical Data[20] with substantially the same result. The adiabatic flame temperature thus calculated was 4370°R, which differs from the reported value by about one percent. The same decomposition products were assumed for PGDN and EN and the calculations were repeated. The results indicate that the adiabatic flame temperature for PGDN is about 5620°R while, for EN, it is about 3590°R.

Bovans[27] has shown that at these temperatures there are appreciable amounts of methane present in the decomposition products. Thus, a more detailed calculation considering the presence of additional components as well as further dissociation would be desirable. However, in light of the approximations and assumptions of the present model, the flame temperatures as calculated above were believed to be justified.

The next property to be determined was the specific heat at constant pressure for the gas phase. As a first approximation, the specific heat for the fuel vapor was estimated using the Dobratz[28] method. Since the products of combustion were known from the flame temperature calculations, the specific heat for the mixture of (assumed) ideal gases comprising the products could also be calculated. The temperature variation of the specific heat from the two methods for PGDN appears in Figure 4.2.

Since the solution of the combustion equations was based on constant properties, a single value for the specific heat had to be determined. To this end, an average film temperature was defined as the average of the maximum and minimum film temperatures. The constant specific heat for the calculations was then taken as the average of the specific heat for the fuel vapor and the products of combustion at the average film temperature. The average specific heat was used since, in region R, the primary constituent is fuel vapor while in region P, the products of combustion predominate.

There are at least two methods available for determining the heat of combustion--the oxygen balance curve[25] and the estimation methods of Reference 28. But for adiabatic burning, an energy balance shows:

$$C_p (T_{f\ ad.} - T_s) = - \Delta H_R - L \quad . \quad (4.26)$$

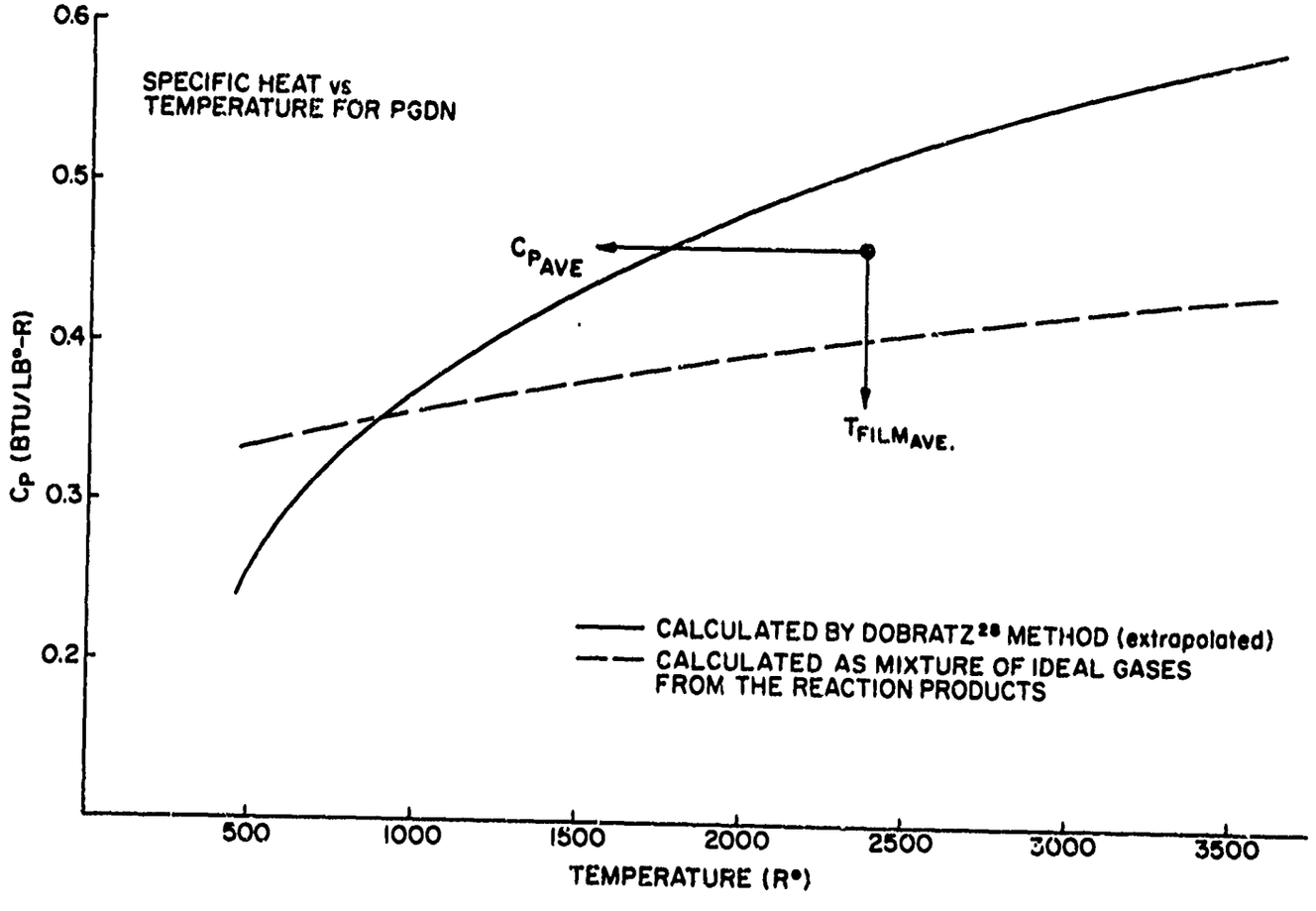

Figure 4.2 Variation of C_p with Temperature for PGDN

Therefore, Equation (4.26) was employed to calculate an effective heat of reaction. The values of the effective heats of reaction were found to roughly coincide with the values from the oxygen balance curve; the maximum difference was about 18 percent.

The values of the remaining properties appear in Appendix B along with the source or method of calculation.

4.2 Combustion Results

In solving the burning equations, one of the input parameters was the experimentally determined radius regression rate $\dot{r}$. Figures 4.3 and 4.4 show the values of $\dot{r}$ as a function of pressure and temperature for PGDN and EN, respectively. Also shown in Figure 4.4 is the strand burning results of Steinberger.[31] It is seen that the droplet burning rates and strand burning rates for EN are of the same order of magnitude at the higher pressures. However, this is probably due to a fortuitous selection of droplet sizes in the present study.

In an attempt to compare the burning rate results with those of Barrere and Moutet,[12] a measurement was made of the burning rate constant for EN and NFN decomposing in a nitrogen atmosphere. The burning rate constant is defined as the slope of the diameter squared versus time curve. At 1200°F and one atmosphere, the burning rate constant for EN was found to be 0.73×10^{-2} cm^2/sec while, in Reference 12, the value was reported as $1.68 \times 10^{-2} cm^2/sec$

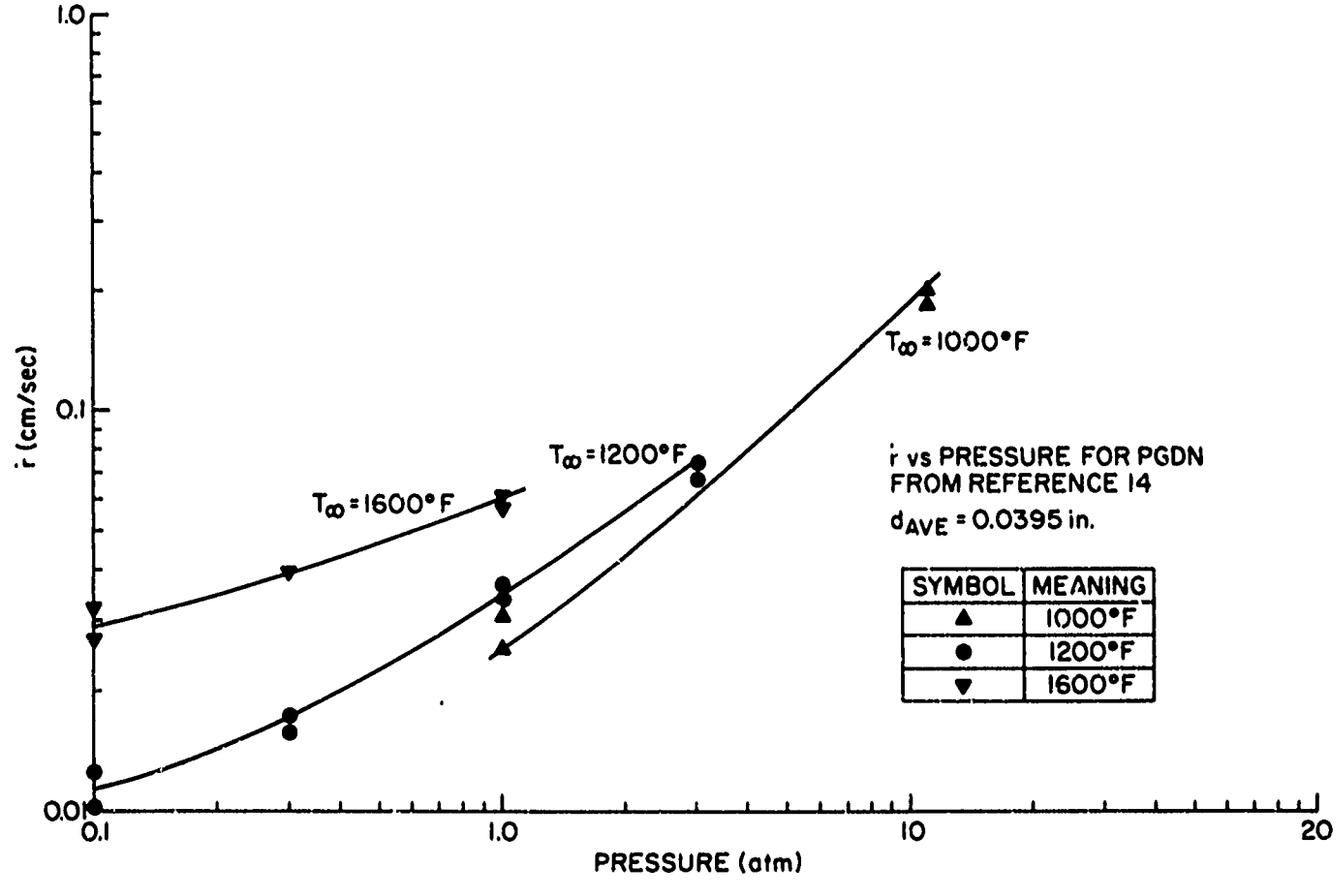

Figure 4.3 Experimental $\dot{r}$ for PGDN

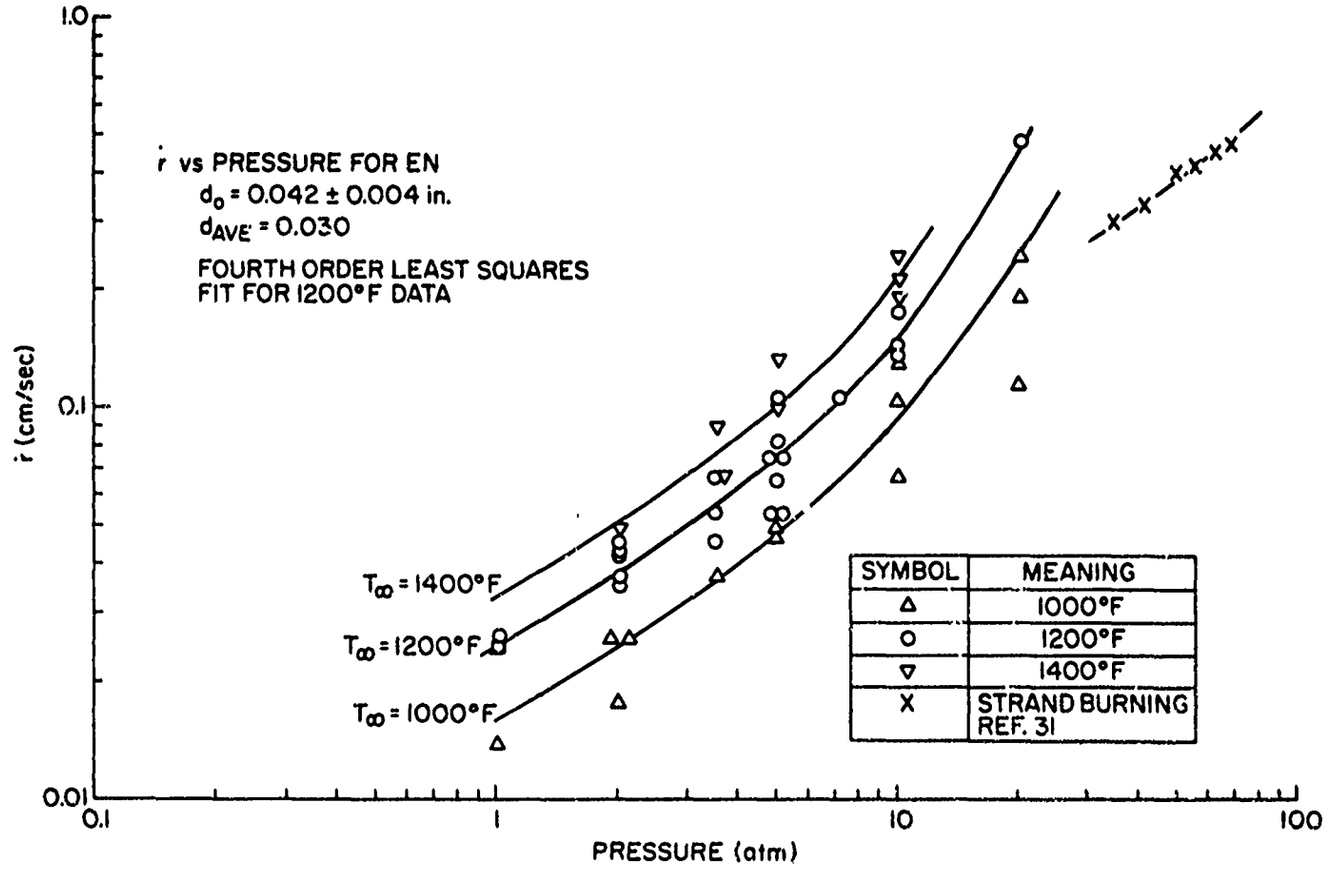

Figure 4.4 Experimental $\dot{r}$ for EN

at the same conditions. For NPN, the measured value was 0.65×10^{-2} cm^2/sec in comparison to the reported value of 1.37×10^{-2} cm^2/sec; the test conditions were identical at $1200^{\circ}F$ and one atmosphere. In addition, Barrere observed a visible flame while luminosity was never observed over the entire test range for EN or NPN in the present investigation. It was found, however, that inflammation could be observed and burning rates could be increased by the introduction of a small amount of air into the chamber. Since Barrere did not evacuate his furnace prior to flooding with nitrogen, as was done in this experiment, it is suggested that some air was present in the furnace during his tests.

The values of the radius regression rate in Figure 4.4 show considerable scatter. The scatter is primarily due to the difficulty in accurately determining the slope of an experimental curve, a process that tends to amplify any experimental errors present in the measurement. The least squares method was employed to correlate the data of Figure 4.4 so that smooth values of $\dot{r}$ could be used in calculating mass transport rates.

The burning rate equations were solved on the IBM 7074 digital computer in the following sequence:

1) Using Equation (4.23) and the measured value of $\dot{r}$, $\dot{m}$ was calculated.
2) σ_∞ was calculated from Equation (4.18).

3) σ_f was calculated from Equation (4.9).

4) θ_f was calculated from Equation (4.10).

5) $\rho_f v_f$ was calculated from Equation (4.24).

Several important characteristics of droplet combustion can be shown from the solution of the burning equations. Figure 4.5 is a plot of dimensionless flame and free stream radii as a function of pressure. This shows quite clearly that these boundaries approach the drop surface (where $\sigma = 1$) as the pressure increases, but the flame position was shown to be a function of the reaction rate. Thus, one may infer that the reaction rate is dependent on pressure.

The inward movement of these boundaries can also be demonstrated by drawing the temperature profiles in the boundary layer as a function of pressure. To this end, Equations (4.5) and (4.6) were put in dimensionless form and used to determine the temperature distribution. Figure 4.6 shows the result of the calculation with temperature being plotted versus radial position in the boundary layer at several pressures. The flame is indicated by the peak temperature while the free stream boundary is characterized by the point where $\theta = 1$. Once again, Figure 4.6 shows the boundaries approach the drop as the pressure increases.

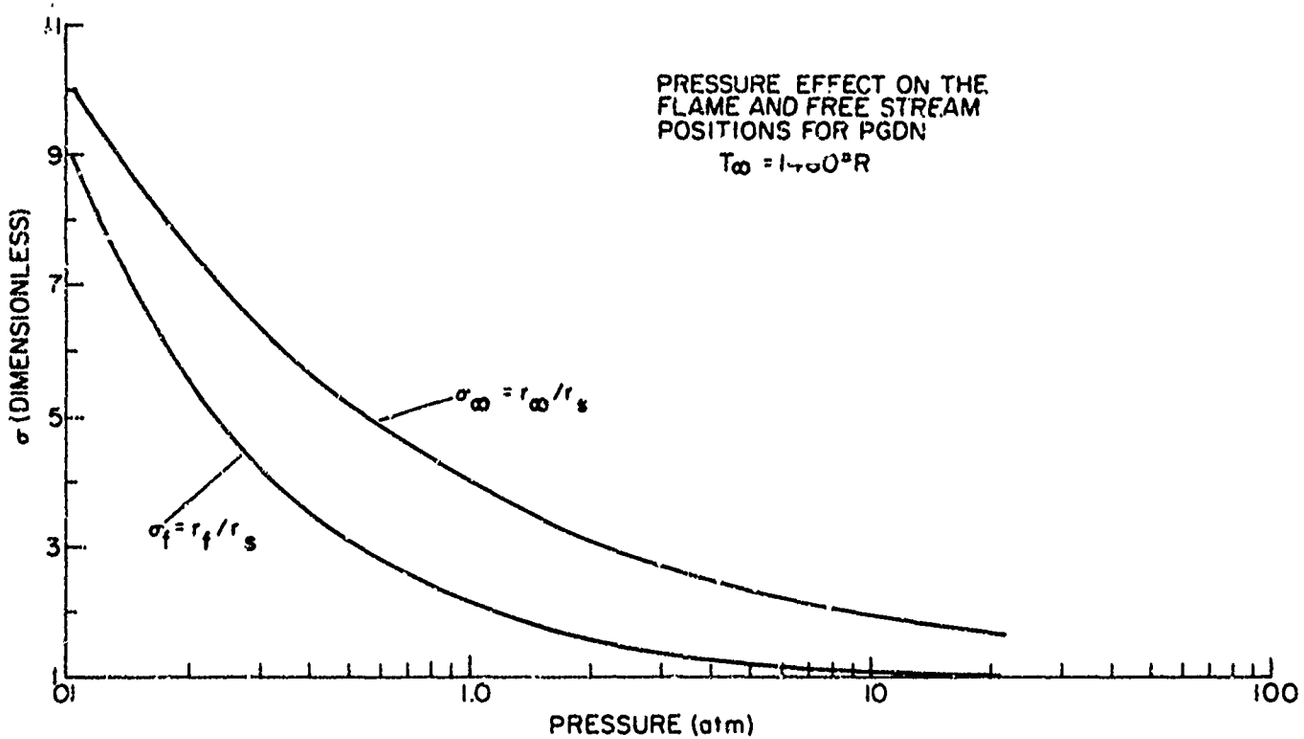

Figure 4.5 Pressure Effect on σ for PGDN

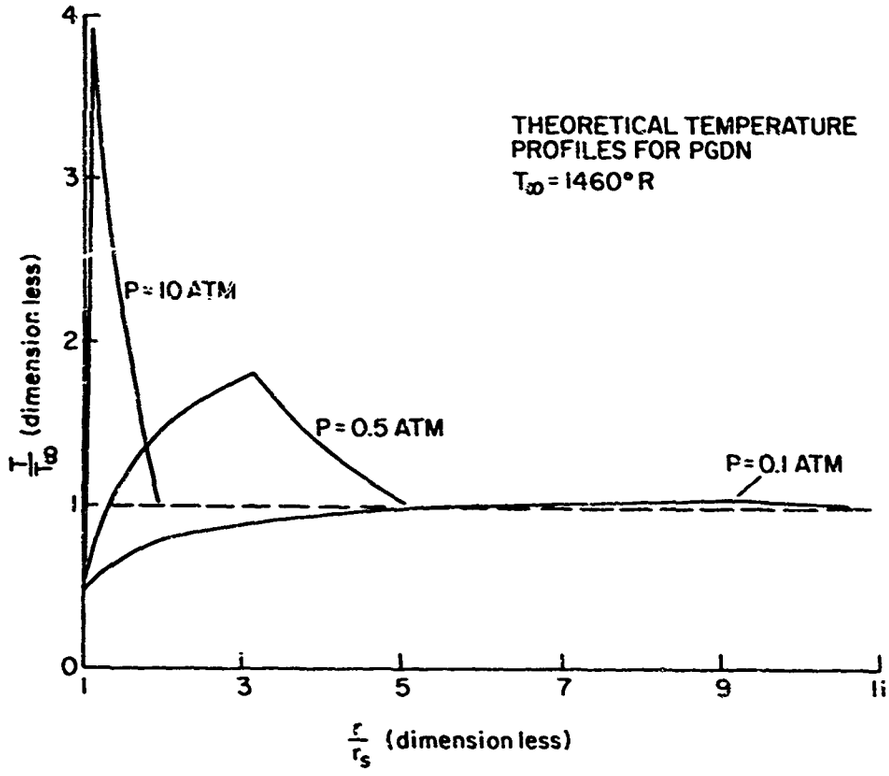

Figure 4.6 Temperature Profiles for PGDN

Figure 4.6 also shows how the temperature gradient at the drop surface increases with pressure. The increased temperature gradient results in higher mass transfer rates at elevated pressure as shown by Equation (4.7).

At high pressure, the flame temperature closely approached the adiabatic flame temperature. Thus, at high pressures, the heat loss to the surroundings appears to be minimized. This is due to the decreased surface area available for heat transfer as the flame moves closer to the droplet. Since the surface area of a sphere is proportional to the radius squared, the flame position strongly affects the heat transfer rate to the surroundings.

As stated before, the flame position is dependent on the rate at which the outward flowing combustible material is reacted. As the pressure increases, the mass transfer rate of the combustible material increases due to the increased temperature gradients at the drop surface. Hence, we may expect the burning rate of the droplet to continually increase. However, the process is somewhat self-controlling since the large mass transfer rates at high pressure tend to sweep back the temperature profile in an effect comparable to ablative cooling.

At high pressure, the burning rate is governed by chemical kinetics; however, at low pressure, the combustion process is much different. Here, the flame is located at some distance from the droplet and its actual position, which is governed by kinetics,

exerts a smaller influence on the burning rate. Since the temperature profiles are much flatter at low pressure, Figure 4.6, the heat transferred to the droplet is lower. This results in lower mass transfer rates and lower burning rates.

As stated previously, the reaction is kinetically controlled at elevated pressure. To demonstrate the kinetic control and infer the order of the reaction, Williams'[15] phenomenological analysis for a propagating flame was employed. The relation for the laminar flame speed may be written:

$$\rho_f v_f = A T_f^{\beta} P^{\frac{n}{2}} \exp(-E/2R_o T_f) \quad , \qquad (4.27)$$

where n is the order of the reaction. By plotting $\ell n\ \rho_f v_f$ against $\ell n\ P$ at constant T_f, the slope of the resulting curve will be an indication of the reaction order. Figure 4.7 is such a plot for PGDN at three values of constant flame temperature. The dashed line is drawn with $n = 1$ and, as can be seen, the data points appear to asymptotically approach the dashed curve at the higher pressures.

Figure 4.8 is a similar plot of $\ell n\ \rho_f v_f$ versus ℓn pressure but for EN. Here, too, the points seem to approach the dashed curve where $n = 1$. However, it is clear that the data of Figures 4.7 and 4.8 do not follow a straight line, the slope of

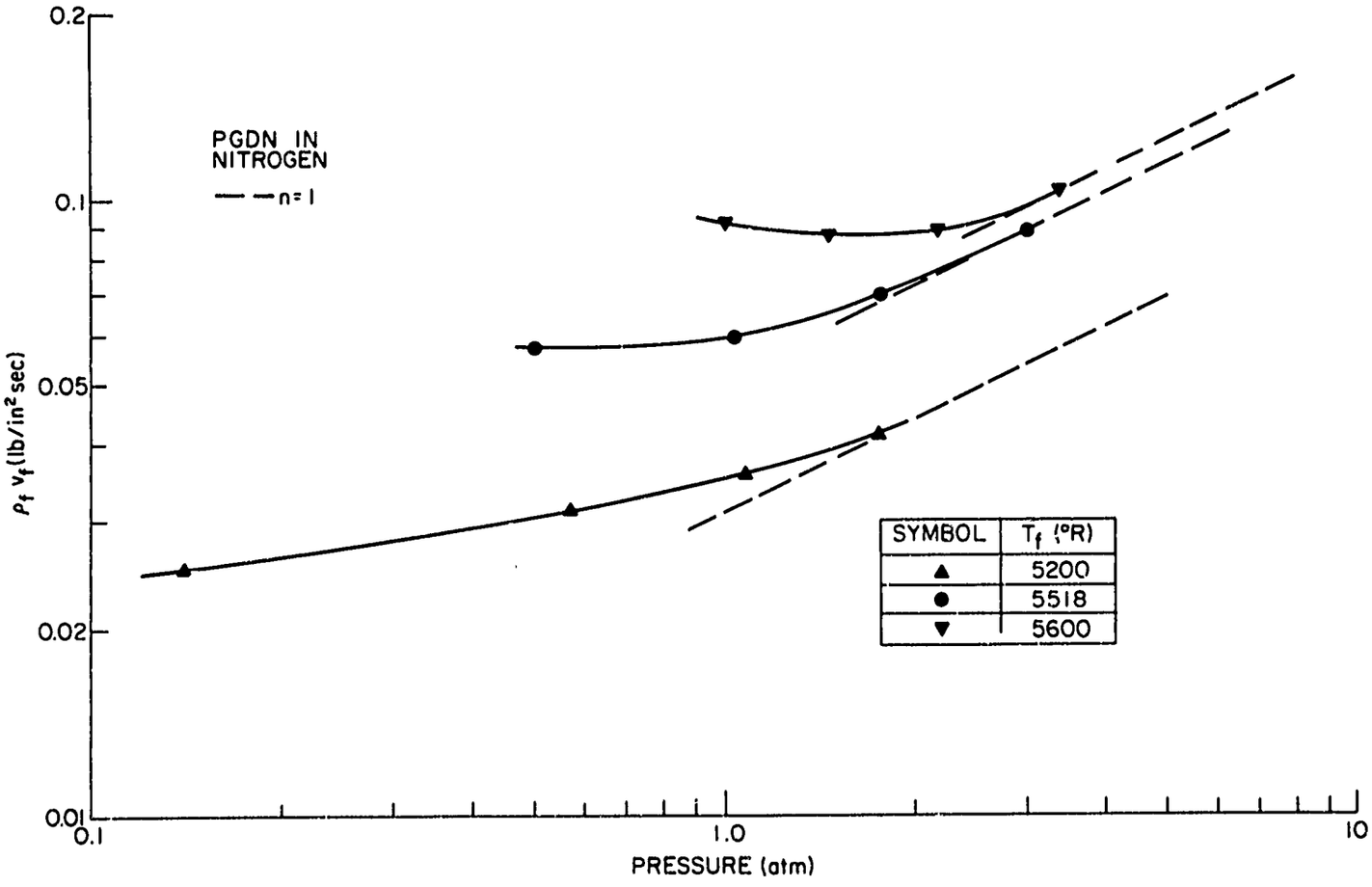

Figure 4.7 Reaction Order for PGDN

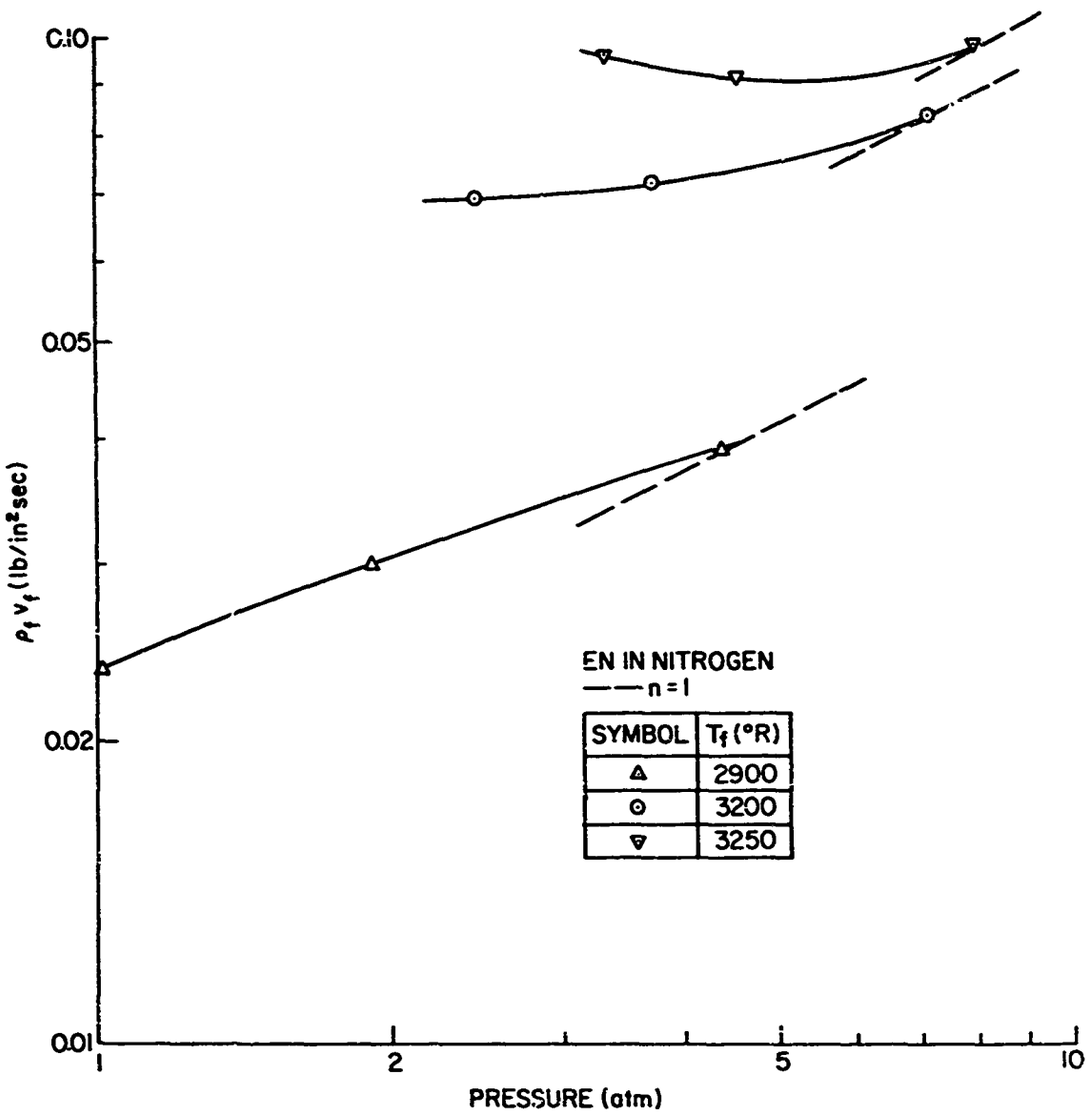

Figure 4.8 Reaction Order for EN

which would indicate the reaction order. This indicates the approximate nature of the combustion model and the difficulty in predicting kinetic parameters from such a model.

The validity of the present simplified combustion model can be further investigated by comparing the computed results to the a priori calculations listed in the literature. To do this, Equation (4.27) was employed to determine the activation energy E from computed values of the laminar flame speed. This was done by plotting $\ell n\ \rho_f\ v_f$ versus $1/T_f$ at constant pressure as shown in Figures 4.9 and 4.10. The temperature dependence is carried primarily by the exponential term and thus the pre-exponential temperature term may be neglected. If the solution were correct, the activation energy E should be near the value reported in the literature from a study of chemical kinetics. The reported value of the activation energy for PGDN was 37.4 K cal/mol,[19] while for EN it was 39.9 K cal/mol.[7] The measured value of E for PGDN, as determined by the slope of a best-fit straight line through the data points of Figure 4.9, was found to be 46 K cal/mol. Also shown in Figure 4.9 is the data from Reference 14 for a realistic thermal conductivity which results in an activation energy of 294 K cal/mol. Thus, it appears that the present model more nearly reflects the actual combustion process since the measured value of activation energy compares favorably with the reported

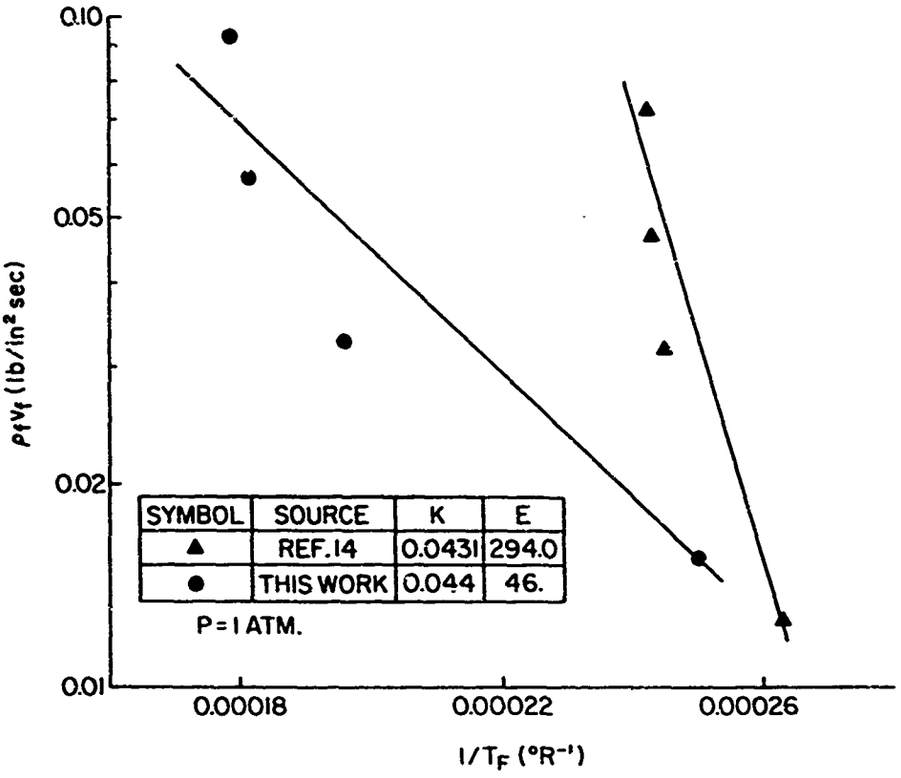

Figure 4.9 Activation Energy for PGDN

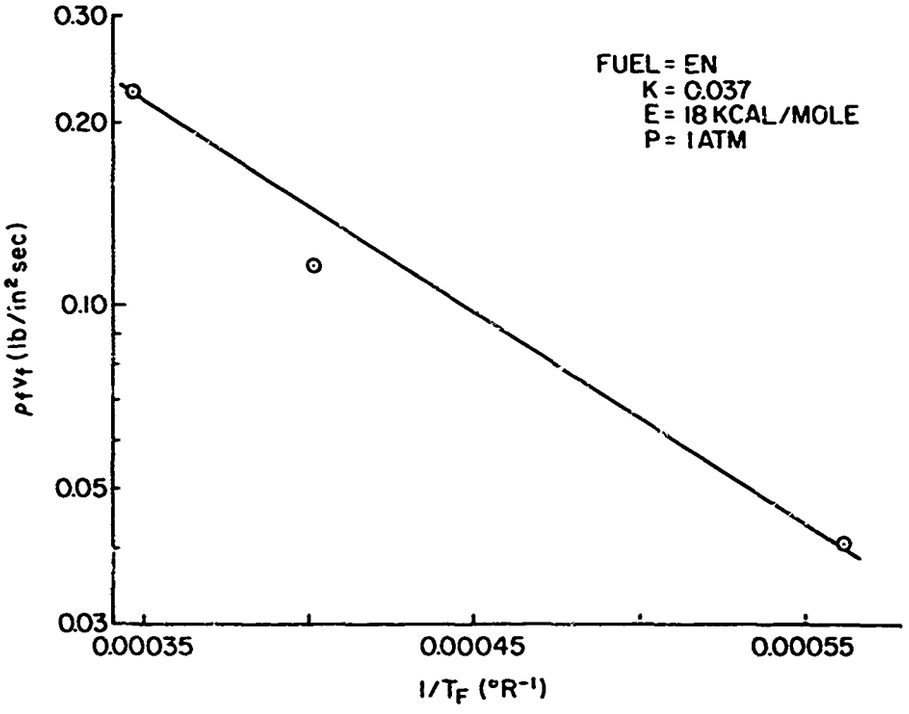

Figure 4.10 Activation Energy for EN

value. It seems quite apparent that the inclusion of natural convection heat losses does account for the difficulties experienced by Karhan.

In addition, the measured activation energy for EN as shown in Figure 4.10 was found to be 18 K cal/mol. This is about 45 percent of the reported value, but at least it is of the same order.

It must be pointed out that the points in Figures 4.9 and 4.10 should plot on a straight line, assuming that Equation (4.27) is valid. The fact that they do not indicates that the analysis is not sufficiently complete; thus, a close inspection of the underlying assumptions seems necessary.

First, the validity of the Ranz and Marshall correlation when applied to a burning droplet is unknown. The solution of the natural convection heat transfer problem for a burning droplet involves a complex boundary condition and the solution apparently has not been reported. Thus, the actual natural convection heat loss may not be truly represented in the present analysis.

The film theory approximation employed here represents only the overall boundary layer and does not consider the existing complex temperature profile. Thus, the value of r_∞ calculated from the film theory approximation may not be representative of the actual r_∞.

The assumption of quasi-steady burning is invalid at high pressure since the liquid temperature constantly increased. In addition, the diameter was constantly decreasing, raising the possibility of transient effects.

Also, the wet bulb assumption is invalid at high pressure since the liquid temperature never reached a value near the wet bulb temperature. An analysis using measured liquid temperatures would undoubtedly reflect actual conditions more realistically.

The constant property assumption is invalid since the temperature of the liquid and gas phases changes considerably as the pressure changes. Thus, an analysis considering the effects of property variations would be desirable.

Finally, the measurement of slopes by graphical methods has always been difficult to perform. The values of the radius regression rate are thus inherently subject to error. The difficulty of slope measurement is also evident in calculating the value of the activation energy.

CHAPTER V

SUMMARY

An investigation of the ignition and decomposition characteristics of nitrate ester monopropellants was undertaken with the specific objectives of the study being:

1) To check the heat-up model proposed by Karhan[14] on several other liquid monopropellants,
2) To explain any discrepancy noted in the ignition results at high pressure,
3) To modify Williams'[15] combustion theory to include the effect of natural convection, and
4) To check the combustion theory thus modified on several other monopropellants.

The experimental apparatus employed here permitted testing at various pressures, temperatures and droplet sizes. The fuels used were propylene glycol dinitrate, ethyl nitrate, nitromethane and normal prypyl nitrate.

The measured ignition times of ethyl nitrate and nitromethane were found to compare favorably with the heat-up model at low pressure. Karhan found a similar agreement for propylene glycol

dinitrate at low pressure and thus the model appears to predict ignition times accurately in this regime.

At high pressure, ignition was detected before the droplet reached its wet bulb temperature and the ignition model results did not agree with measured ignition times. In this case, it was found that the ignition event would correlate with an ignition temperature concept. However, the ignition temperatures employed were probably valid only for the test range encountered in the present study. This indicates a need for further monopropellant ignition studies at states other than the wet bulb state.

The combustion theory was modified to include natural convection heat losses during non-adiabatic burning. The familiar film theory approximation was used to predict an effective boundary layer thickness while the actual heat transfer characteristics were correlated by the empirical formulation of Ranz and Marshall.[26] Since there was a flamelike appearance in the boundary layer, the Grashof number appearing in the empirical formulation was modified to account for the high temperature, low density gases in the flame zone.

The combustion model thus modified was checked on propylene glycol dinitrate and ethyl nitrate using measured values of the radius regression rate. It was found that the inclusion of natural convection resulted in activation energies of the order reported in the literature using realistic properties.

The differences between the measured and reported values of the activation energies may be due to several factors. First, the measurement of the slope of the diameter versus time plots was subject to error. This resulted in a scatter of the radius regression rate which is an input to the solution of the burning equations. Thus, it would be desirable to check the combustion model using additional radius regression rate data.

Secondly, the plot of $\ell n\ \rho_f\ v_f$ versus $1/T_f$ was a curve and the choice of a best-fit straight line through the points may be questionable. In addition, the fact that the points are not a straight line suggests an investigation into the underlying assumptions of the model.

In addition, all of the properties used were assumed constant. Since there are significant temperature changes in the boundary layer, the constant property solution can be expected to produce only approximate results. Undoubtedly, a variable property solution would be more realistic and would determine the errors caused by the assumption of constant properties.

A comparison was made between the burning rate constants of this work and those of Barrere and Moutet.[12] The result showed the present values to be roughly one-half of those from Reference 12. It was also found that a luminous flame could be observed with a resulting increase in burning rate by admitting a small amount of

air to the test chamber of the present experiment. Thus, it is suggested that some air was present in the furnace during the tests of Barrere and Moutet.

Finally, an attempt was made to infer kinetic parameters from the computed laminar flame speeds. Although the results indicated an asymptotic approach to a first-order reaction, no general conclusions can be made since the points did not fall on a straight line.

BIBLIOGRAPHY

1. Lawver, B. R. "Some Observations on the Combustion of N_2H_4 Droplets," AIAA Paper No. 65-355, (1965).

2. Hottel, H. C., Williams, G. C., and Simpson, H. R., "Combustion of Drops of Heavy Liquid Fuels," 5th Symposium on Combustion, Reinhold, New York, pp. 101-124 (1955).

3. Kobayasi, K., "An Experimental Study on the Combustion of a Fuel Droplet," 5th Symposium on Combustion, Reinhold, New York, pp. 141-148 (1955).

4. Nishiwaki, N., "Kinetics of Liquid Combustion Processes: Evaporation and Ignition Lag of Fuel Droplets," 5th Symposium on Combustion, Reinhold, New York, pp. 148-158 (1955).

5. Faeth, G. M., "The Kinetics of Droplet Ignition in a Quiescent Air Environment," (The Pennsylvania State University, Ph.D. thesis, Department of Mechanical Engineering, 1964).

6. Priem, R. I., and Heidmann, M. F., "Propellant Vaporization as a Design Criterion for Rocket-Engine Combustion Chambers," NASA Technical Report R-67 (1960).

7. Adams, G. K., and Bawn, C. E. H., "The Homogeneous Decomposition of Ethyl Nitrate," Trans. of the Faraday Soc. 45, 494-499 (1949).

8. Phillips, L., "The Pyrolysis of Methyl Nitrate," J. Chem. Soc., 3082-3090 (1960).

9. Faeth, G. M., "Monopropellant Droplet Burning at Low Reynolds Numbers," Combustion and Flame 11, No. 2, 167-174 (1967).

10. Levy, J. B., "The Thermal Decomposition of Nitrate Esters. 1. Ethyl Nitrate," J. Chem. Soc. 76, 3254-3257 (1954)

11. Phillips, L., "Thermal Decomposition of Organic Nitrates," Nature, 165, 564 (1950).

12. Barrere, M., and Moutet, H., "Etude Experimentale de la Combustion de Gouttes de Monergal," La Recherche Aeronautique, 50, 31-38, March-April (1956)

13. Rosser, W. A., "The Decomposition Burning of Monopropellant Drops: Hydrazine, Nitromethane and Ethyl Nitrate," Prog. Rept. 20-305, California Institute of Technology, Jet Propulsion Laboratory, Pasadena, California (1957).

14. Karhan, B., "The Ignition and Combustion of a Liquid Monopropellant," (The Pennsylvania State University, M.S. thesis, Department of Mechanical Engineering, 1967).

15. Williams, F. A., Combustion Theory, (Addison-Wesley Publishing Company, Inc., New York, 1958, pp. 231-249).

16. Handbook of Chemistry and Physics, 47th edition, Chemical Rubber Publishing Company, Cleveland, Ohio, p. D-138 (1966-67).

17. Crater, E. de C., "The Vapor Pressure of Glycerol Trinitrate and Certain Glycol Dinitrates," Ind. Eng. Chem. 21, 674-676 (1929).

18. Gray, P. and Pratt, M. W. T., "The Latent Heats of Vaporization of the Alkyl Nitrates," J. Chem. Soc., 2163-2168 (1957).

19. Phillips, L., "Thermal Decomposition of Organic Nitrates," Nature 160, 753-754 (1947).

20. JANAF Thermochemical Data, The Dow Chemical Company, Thermal Laboratory, Midland, Michigan (1961).

21. Spalding, D. B., and Jain, V. K., "Theory of the Burning of Monopropellant Droplets," A. R. C. Technical Report Number 20-176, Current Paper Number 447 (1958).

22. Beilstein's Handbuch Der Organischem Chemie, (4 Auflant Band 1 Sweiter Teil, Springer-Verlag, Berlin, 1958, p. 2149).

23. Beilstein's Handbuch Der Organischem Chemie, Volume I, (4 Auflant Band 1 Sweiter Teil, Springer-Verlag, Berlin, 1958, p. 329).

24. Beilstein's Handbuch Der Organischem Chemie, Volume III, B. D. 1-Supp. 2, (4 Auflant Band 1 Sweiter Teil, Springer-Verlag, Berlin, 1958, p. 40).

25. Altman, D., Carter, J. M., Penner, S. S., and Summerfield, M., Liquid Propellant Rockets, (Princeton University Press, Princeton, New Jersey, 1960, pp. 87-89).

26. Ranz, W. E. and Marshall, W. R., "Evaporation from Drops," Chem. Eng. Prog. 48, pp. 141-180 (1952).

27. Bovans, R. S., "Technical Information Concerning Normal Propyl Nitrate," Report No. RM-118, Ethyl Corporation, Detroit, Michigan (1954).

28. Reid, R. C., and Sherwood, T. K., The Properties of Gases and Liquids, (McGraw-Hill Book Company, Inc., New York, 1958).

29. Eckert, E. R. G., and Drake, R. M., Heat and Mass Transfer, (McGraw-Hill Book Company, Inc., New York, 2nd edition, 1959, pp. 474-506).

30. Spalding, D. B., "The Combustion of Liquid Fuels," Fourth Symposium (International) on Combustion, The Williams and Wilkins Company, pp. 855 (1953).

31. Steinberger, "Mechanism of Burning Nitrate Esters," Fifth Symposium on Combustion, Reinhold, New York, p. 209 (1955).

32. Gray, P., and Smith, P. L., "Low-Temperature Calorimetry and the Thermodynamic Properties of Ethyl Nitrate," J. Chem. Soc., 769-773 (1954).

APPENDIX A

DERIVATION OF THE COMBUSTION EQUATIONS

With the assumptions and terminology of Chapter IV, the conservation of mass principle applied to a control volume bounded by spheres of radius r and $r + dr$ yields:

$$\frac{d}{dr}\left(r^2 \dot{m}''\right) = 0 \quad . \tag{A.1}$$

This equation can be readily integrated with the result being:

$$r^2 \dot{m}'' = \text{constant} \quad . \tag{A.2}$$

The steady-flow energy equation applied to a similar control volume shows:

$$r^2 \dot{m}'' C_p \frac{dT}{dr} - \frac{d}{dr}\left(r^2 K \frac{dT}{dr}\right) = 0 \quad . \tag{A.3}$$

Rearranging and integrating Equation (A.3) twice, the result is:

$$T = C_1 + C_2 \exp\left(-a/r\right) \quad , \tag{A.4}$$

where C_1 and C_2 are the two constants of integration and a is defined by the grouping:

$$a = r_s^2 \dot{m}_s'' C_p/K \quad . \tag{A.5}$$

Equation (A.4) applies to the reactants between the drop surface and the flame (region R) and to the products of combustion between the flame and the free stream (region P). The value of the

constants C_1 and C_2 will be different for each region. To evaluate the constants, the boundary conditions must be employed. In region R,

$$T = T_s \quad \text{at} \quad r = r_s \tag{A.6}$$

$$T = T_f \quad \text{at} \quad r = r_f \quad . \tag{A.7}$$

Applying the boundary conditions in region R yields:

$$C_{1_R} = T_s - \frac{(T_s - T_f) \exp(-a/r_s)}{\exp(-a/r_s) - \exp(-a/r_f)}$$

$$C_{2_R} = (T_s - T_f) / [\exp(-a/r_s) - \exp(-a/r_f)] \quad . \tag{A.8}$$

In region P , the boundary conditions are as follows:

$$T = T_f \quad \text{at} \quad r = r_f \tag{A.9}$$

$$T = T_\infty \quad \text{at} \quad r = r_\infty \quad . \tag{A.10}$$

By comparing these boundary conditions to those in region R, it is evident that the same solution for the constants results if the subscripts s and f are replaced by f and ∞ , respectively. In final form, the energy equation in region R yields:

$$T = \frac{T_f \exp(-a/r_s) - T_s \exp(-a/r_f) + (T_s - T_f) \exp(-a/r)}{\exp(-a/r_s) - \exp(-a/r_f)} \quad .$$

(A.11)

Similarly, the solution of the energy equation in region P results in the following:

$$T = \frac{T_\infty \exp(-a/r_f) - T_f \exp(-a/r_\infty) + (T_f - T_\infty)\exp(-a/r)}{\exp(-a/r_f) - \exp(-a/r_\infty)} \quad . \tag{A.12}$$

At this point, it would be desirable to have a relationship to determine r_f, r_∞ and T_f. With the wet bulb assumption, all the heat transferred to the droplet is utilized as the latent heat of vaporization. Thus, the energy equation applied at the drop surface shows:

$$K \left.\frac{dT}{dr}\right|_{r_s} = \dot{m}'' L \quad . \tag{A.13}$$

Differentiating Equation (A.11) to obtain the temperature gradient, substituting into Equation (A.13) and rearranging yields:

$$\frac{a}{r_s}\left(\frac{1}{r_s} - \frac{1}{r_f}\right) = \ell n\left[1 + \frac{C_p (T_f - T_s)}{L}\right] \quad . \tag{A.14}$$

This equation can be put into dimensionless form by defining the following parameters:

$$\begin{aligned} \sigma &= r/r_s \\ \theta &= T/T_\infty \\ \alpha &= L/C_p T_\infty \quad . \end{aligned} \tag{A.15}$$

With these substitutions, Equation (A.14) may be rewritten in dimensionless form as follows:

$$\frac{a}{r_s}\left(1 - \frac{1}{\sigma_f}\right) = \ell n \left[1 + \frac{\theta_f - \theta_s}{\alpha}\right] \quad . \qquad (A.16)$$

With the thin flame assumption, the energy equation applied to a thin spherical shell enclosing the flame results in the following:

$$-K \left.\frac{dT}{dr}\right|_{r_f^-} + \dot{m}_f'' \, h_R\,(T_f) = -K \left.\frac{dT}{dr}\right|_{r_f^+} + \dot{m}_f'' \, h_p\,(T_f) \quad . \qquad (A.17)$$

Equations (A.11) and (A.12) may be differentiated to obtain the temperature gradients for Equation (A.17). Letting

$$\Delta H_R = h_p\,(T_f) - h_R\,(T_f) \quad , \qquad (A.18)$$

substituting the gradients into Equation (A.17) and rearranging results in:

$$\frac{(T_s - T_f)\exp\left[a\left(\frac{1}{r_s} - \frac{1}{r_f}\right)\right]}{1 - \exp\left[a\left(\frac{1}{r_s} - \frac{1}{r_f}\right)\right]} = \frac{T_f - T_\infty}{1 - \exp\left[a\left(\frac{1}{r_f} - \frac{1}{r_\infty}\right)\right]} - \frac{\Delta H_R}{C_p} \quad . \qquad (A.19)$$

T_f may be found explicitly by substituting Equation (A.14) into Equation (A.19). The result of this substitution is:

$$T_f = T_s - \frac{L}{C_p} - \frac{\Delta H_R}{C_p} + \left(T_\infty + \frac{L}{C_p} + \frac{\Delta H_R}{C_p} - T_s\right) \exp\left[-a\left(\frac{1}{r_f} - \frac{1}{r_\infty}\right)\right] \quad . \tag{A.20}$$

In dimensionless form, this equation becomes:

$$\theta_f = \theta_s - \alpha - Q + (1 + \alpha + Q - \theta_s) \exp\left[-\frac{a}{r_s}\left(\frac{1}{\sigma_f} - \frac{1}{\sigma_\infty}\right)\right] \quad , \tag{A.21}$$

where

$$Q = \Delta H_R/(C_p T_\infty) \quad . \tag{A.22}$$

The next variable to be determined is the dimensionless free stream radius σ_∞. The problem is to find an effective σ_∞ when the actual boundary layer is replaced by a stagnant boundary layer with the same temperature at the drop surface and at the free stream. This is the familiar film theory approximation. The terminology for the derivation is as follows:

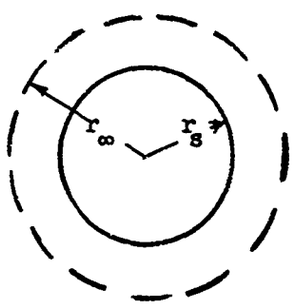

Under the film theory approximation and neglecting mass transfer, the energy equation applied to the control volume bounded by spheres of radius r_s and r_∞ yields:

$$\frac{d}{dr}\left(r^2 \frac{dT}{dr}\right) = 0 \quad . \tag{A.23}$$

This equation may be integrated twice to produce the following result:

$$T = C_3 + C_4/r \quad , \tag{A.24}$$

where C_3 and C_4 are two arbitrary constants of integration. The boundary conditions for this model are:

$$\begin{aligned} T &= T_s \quad \text{at} \quad r = r_s \\ T &= T_\infty \quad \text{at} \quad r = r_\infty \quad . \end{aligned} \tag{A.25}$$

Thus, Equations (A.25) may be employed to evaluate the constants C_3 and C_4. By carrying out these details, Equation (A.24) becomes:

$$T = T_s + \frac{T_\infty - T_s}{r_s\left(\frac{1}{r_s} - \frac{1}{r_\infty}\right)} + \frac{T_\infty - T_s}{r\left(\frac{1}{r_\infty} - \frac{1}{r_s}\right)} \quad . \tag{A.26}$$

The heat transferred to the droplet at the surface takes place by conduction and, hence, this may be expressed by the Fourier conduction law as:

$$\dot{q}'' = K \left.\frac{dT}{dr}\right|_{r_s} \quad . \tag{A.27}$$

The heat transferred through the boundary layer is just equal to that conducted to the droplet and may be expressed by Newton's law of cooling as:

$$\dot{q}'' = h_c \, (T_\infty - T_s) \quad . \tag{A.28}$$

The temperature gradient at the drop surface $\left.\frac{dT}{dr}\right|_{r_s}$ may be evaluated from Equation (A.26). Making this substitution in Equation (A.27) and equating the heat fluxes results in:

$$\frac{h_c}{K} = \frac{1}{r_s^2 \left(\frac{1}{r_s} - \frac{1}{r_\infty}\right)} \quad . \tag{A.29}$$

The dimensionless Nusselt number relates convection heat transfer to conduction heat transfer and may be stated as:

$$Nu = \frac{h_c \, d_s}{K} \quad . \tag{A.30}$$

Substituting Equation (A.29) into Equation (A.30) and introducing the dimensionless radius from Equations (A.15) results in:

$$\sigma_\infty = \frac{Nu}{Nu - 2} \quad . \tag{A.31}$$

The Nusselt number for the actual heat transfer process was calculated from the Ranz and Marshall[26] correlation for heat transfer to drops. This may be expressed as follows:

$$Nu = 2 + 0.6 \, Pr^{1/3} \, Gr^{1/4} \quad . \tag{A.32}$$

The dimensionless flame radius may be found explicitly by substituting Equation (A.21) into Equation (A.16). The result of this substitution is:

$$\sigma_f = a/r_s \left\{ \frac{a}{r_s} + \ell n \left[\frac{1 + \alpha + Q - \theta_s}{Q} \exp\left(\frac{a}{r_s \sigma_\infty} - \frac{a}{r_s} \right) - \frac{\alpha}{Q} \right] \right\} \quad . \tag{A.33}$$

Finally, for quasi-steady burning, the conservation of mass principle yields:

$$\rho_f v_f = \dot{m}/(4 \pi r_s^2 \sigma_f^2) \quad . \tag{A.34}$$

APPENDIX B

LIQUID AND GAS PROPERTIES

LIQUID AND GAS PROPERTIES

B-1 Liquid Properties (at 77°F and low pressure)

For PGDN $C_3H_6(NO_3)_2$

Property	Value	Source or Calculation Method
Density	86 lb/ft^3	Beilstein,[22] de. C. Crator[17]
Specific heat	0.414 BTU/lb °R	calc-Johnson and Huang[28] method
Latent heat	158 BTU/lb	calc-Giacalone[28] method
Critical pressure	35.8 Atm	calc-Lyderson[28] method
Critical temperature	1070 °R	From vapor pressure curve at critical pressure
Thermal conductivity	0.095 $\frac{\text{BTU}}{\text{hr ft °R}}$	calc-Weber[28] method
Heat of reaction	2378 BTU/lb	From Equation (4.12)

LIQUID AND GAS PROPERTIES

B-1 Liquid Properties (at 77°F and low pressure)

For EN $C_2H_5NO_3$

Property	Value	Source or Calculation Method
Density	68.5 lb/ft^3	Beilstein[23]
Specific heat	0.44 B/lb °R	Gray and Smith[32]
Latent heat	172 B/lb	Gray and Pratt[18]
Critical pressure	48.3 Atm	calc-Lyderson[28] method
Critical temperature	975 °R	calc-Lyderson[28] method
Thermal conductivity	0.0967 $\frac{BTU}{hr\ ft\ ^\circ R}$	calc-Weber[28] method
Heat of reaction	1458 BTU/lb	From Equation (4.12)

LIQUID AND GAS PROPERTIES

B-1 Liquid Properties (at 77°F and low pressure)

For NM CH_3NO_2

Property	Value	Source or Calculation Method
Density	71 lb/ft^3	Beilstein[24]
Specific heat	0.412 BTU/lb °R	Handbook of Chemistry and Physics[16]
Latent heat	290 BTU/lb	Gray and Pratt[18]
Critical pressure	63.9 Atm	calc-Lyderson[28] method
Critical temperature	1070 °R	calc-Lyderson[28] method
Thermal conductivity	0.1244 $\frac{\text{BTU}}{\text{hr ft °R}}$	Handbook of Chemistry and Physics[16]
Heat of reaction	1710 BTU/lb	From Equation (4.12)

LIQUID AND GAS PROPERTIES

B-2 Gas Properties (at low pressure)

For PGDN (at T = 2070°F)

Property	Value	Source or Calculation Method
Specific heat	0.463 BTU/lb	From Figure 4.2
Thermal conductivity	$0.0440 \frac{\text{BTU}}{\text{hr ft } ^{\circ}\text{R}}$	Eckert and Drake[29]
Absolute viscosity	$32.7 \times 10^{-6} \frac{\text{lb}}{\text{ft sec}}$	Eckert and Drake[29]

LIQUID AND GAS PROPERTIES

B-2 Gas Properties (at low pressure)

For EN (at T = 1410°F)

Property	Value	Source or Calculation Method
Specific heat	0.505 BTU/lb	calc-Dobratz[28] method
Thermal conductivity	$0.0370 \frac{\text{BTU}}{\text{hr ft } ^{\circ}\text{R}}$	Eckert and Drake[29]
Absolute viscosity	$27.5 \times 10^{-6} \frac{\text{lb}}{\text{ft sec}}$	Eckert and Drake[29]

LIQUID AND GAS PROPERTIES

B-2 Gas Properties (at low pressure)

For NM (at $T = 1330^{\circ}F$)

Property	Value	Source or Calculation Method
Specific heat	0.405 BTU/lb	calc-Dobratz[28] method
Thermal conductivity	$0.0374 \frac{BTU}{hr\ ft\ ^{\circ}R}$	Eckert and Drake[29]
Absolute viscosity	$26.88 \times 10^{-6} \frac{lb}{ft\ sec}$	Eckert and Drake[29]